



eLIFE

Sheraton House
Castle Park
Cambridge CB3 0AX, UK

P 01223 370155
W elifesciences.org
T @elifesciences

IN PRESS

The rise and fall of the *Phytophthora infestans* lineage that triggered the Irish potato famine

The late blight pandemic that included the Irish Great Famine in the nineteenth century was caused by a single *Phytophthora infestans* genotype, which is distinct but closely related to the most prevalent genotype of the twentieth century.

Kentaro Yoshida (The Sainsbury Laboratory), Verena Schuenemann (University of Tübingen), Liliana Cano (The Sainsbury Laboratory), Marina Pais (The Sainsbury Laboratory), Bagdevi Mishra (Biodiversity and Climate Research Centre), Rahul Sharma (Biodiversity and Climate Research Centre), Christa Lanz (Max Planck Institute for Developmental Biology), Frank Martin (United States Department of Agriculture), Sophien Kamoun (The Sainsbury Laboratory), Johannes Krause (University of Tübingen), Marco Thines (Biodiversity and Climate Research Centre), Detlef Weigel (Max Planck Institute for Developmental Biology), and Hernán Burbano (Max Planck Institute for Developmental Biology)

Abstract:

Phytophthora infestans, the cause of potato late blight, is infamous for having triggered the Irish Great Famine in the 1840s. Until the late 1970s, *P. infestans* diversity outside of its Mexican center of origin was low, and one scenario held that a single strain, US-1, had dominated the global population for 150 years; this was later challenged based on DNA analysis of historical herbarium specimens. We have compared the genomes of 11 herbarium and 15 modern strains. We conclude that the nineteenth century epidemic was caused by a unique genotype, HERB-1, that persisted for over 50 years. HERB-1 is distinct from all examined modern strains, but it is a close relative of US-1, which replaced it outside of Mexico in the twentieth century. We propose that HERB-1 and US-1 emerged from a metapopulation that was established in the early 1800s outside of the species' center of diversity.

<http://dx.doi.org/10.7554/elifesciences.00731>

Please address questions to media@elifesciences.org. Details on how to cite *eLife* articles in news stories and our media policy are available at <http://www.elifesciences.org/news/for-the-press>. Articles published in *eLife* may be read on the journal site at <http://elifesciences.org>.

To be notified of new content at *eLife*, sign up at <http://elifesciences.org>.

34 **Introduction**

35 Potato late blight's impact on humankind is rivaled by few other plant diseases. The Spanish
36 introduced Europeans to the South American staple crop potato shortly after their conquest of
37 the New World, but for three centuries Europe stayed free of *P. infestans*, the causal agent of
38 late blight. In 1845, the oomycete *P. infestans* finally reached Europe, spreading rapidly from
39 Belgium to other countries of mainland Europe and then to Great Britain and Ireland. The
40 impact of the epidemic reached catastrophic levels in Ireland, where the population was more
41 dependent on potato for their subsistence than in other parts of Europe (Bourke, 1964;
42 Reader, 2009). The subsequent Great Famine killed around one million people, and an
43 additional million were forced to leave the island (Turner, 2005). Even today, the Irish
44 population remains less than three quarters of what it was at the beginning of the 1840s.
45 These dramatic consequences of the *P. infestans* epidemic were due to the absence of
46 chemical and genetic methods to combat it; such means became available only several
47 decades later.

48 Ever since triggering the Irish famine, *P. infestans* has continued to wreak havoc on
49 potato fields throughout the world. Late blight remains the most destructive disease of the
50 third largest food crop, resulting in annual losses of potatoes that would be sufficient to feed
51 anywhere from 80 to many hundreds of millions of people (Fisher et al., 2012). *Phytophthora*
52 *infestans* is an extraordinarily virulent and adaptable pathogen (Fry, 2008; Haas et al., 2009).
53 In agricultural systems, sexual reproduction may trigger explosive population shifts that are
54 driven by the emergence and migration of asexual lineages (Cooke et al., 2012; Fry et al.,
55 2009; Fry et al., 1992). The species is thought to originate from Toluca Valley, Mexico,
56 where it infects wild relatives of potato, frequently undergoes sexual reproduction and co-
57 occurs with the two closely related species *P. mirabilis* and *P. ipomoeae* (Flier et al., 2003;
58 Goodwin et al., 1994; Grünwald and Flier, 2005; Tooley et al., 1985). In its center of origin,
59 *P. infestans* is characterized by high levels of genetic and phenotypic diversity (Grünwald and
60 Flier, 2005).

61 The genomes of a few *P. infestans* strains have been described (Cooke et al., 2012;
62 Haas et al., 2009; Raffaele et al., 2010a). Compared to other species in the genus, the 240 Mb
63 T30-4 reference genome of *P. infestans* is large, with three quarters of the genome consisting
64 of repetitive DNA. A large number of genes codes for effector proteins, many of which are
65 delivered inside plant cells to promote host colonization, for instance by suppressing plant
66 immunity. RXLR proteins, the main class of host-translocated effectors, are encoded by about

67 550 genes in the *P. infestans* T30-4 genome. RXLR effectors that can be recognized by plant
68 immune receptors, known as Resistance (R) proteins, are said to have “avirulence” activity.
69 Upon introduction of a cognate *R* gene into the host population, such avirulence effectors
70 become a liability for the pathogen, and natural selection favors the spread of pseudogenized
71 or mutated alleles (Vleeshouwers et al., 2011).

72 The detailed descriptions and drawings of Heinrich Anton de Bary and the reports of
73 several other pioneers of plant pathology leave no doubt that the nineteenth century blight
74 epidemic was triggered by *P. infestans* (Bourke, 1964; de Bary, 1876). What remains
75 controversial is the relationship of the nineteenth century strains to modern isolates. The quest
76 for understanding the origin of the strain that resulted in the Irish famine began with extant
77 samples. Prior to the late 1970s, global *P. infestans* populations outside of South America and
78 Mexico, the centers of diversity of the host and the pathogen, were dominated by a single
79 clonal lineage that had the mitochondrial (mtDNA) haplotype Ib and was called US-1
80 (Goodwin et al., 1994). It was therefore proposed that the US-1 lineage was a direct
81 descendant of the strain that first caused widespread late blight in North America from 1843
82 on, and then triggered the Irish famine beginning in 1845 (Bourke, 1964; Goodwin et al.,
83 1994). This hypothesis was subsequently directly addressed by PCR analysis of infected
84 nineteenth century potato leaves stored in herbaria. The conclusion from these studies was
85 that the historic strains belonged to a mtDNA haplotype, Ia, that was distinct from that of the
86 US-1 lineage (May and Ristaino, 2004; Ristaino et al., 2001). Because Ia was at the time not
87 only the predominant haplotype in the Toluca Valley in Mexico (Flier et al., 2003; Gavino
88 and Fry, 2002), but had also been found in South America (Perez et al., 2001), May and
89 Ristaino (2004) speculated that the nineteenth century and US-1 lineages represented two
90 independent epidemics of divergent lineages that had both originated in South America and
91 spread from there to North America and Europe. A caveat was that these far-reaching
92 conclusions were based on only three mtDNA SNPs (May and Ristaino, 2004; Ristaino et al.,
93 2001).

94 Since these first herbarium analyses, the retrieval and sequencing of DNA from
95 museum specimens, fossil remains and archaeological samples – collectively known as
96 ancient DNA (aDNA) (Pääbo et al., 2004) – have seen impressive advances thanks to the
97 advent of high-throughput sequencing technologies. The combined analysis of modern and
98 ancient genomes of human pathogens has begun to solve important questions about their
99 history and evolution (Bos et al., 2011; Bos et al., 2012). Here we show that aDNA methods

100 hold similar promise for plant pathology and that they can improve our understanding of
101 historically important plant pathogen epidemics.

102 To determine how the historic *P. infestans* strain(s) relate to extant isolates, we
103 shotgun-sequenced 11 herbarium samples of infected potato and tomato leaves collected from
104 continental Europe, Great Britain, Ireland, and North America in the period from 1845 to
105 1896, and extracted information on *P. infestans* mitochondrial and nuclear genomes. To
106 understand the subsequent evolution of the pathogen, we compared the historic *P. infestans*
107 genomes to those of 15 modern twentieth century strains that span the genetic diversity of the
108 species, and to the two sister species *P. ipomoeae* and *P. mirabilis*. Our analyses revealed that
109 the nineteenth century epidemic was caused by a single genotype, HERB-1, that persisted for
110 at least 50 years. While it is distinct from all examined modern strains, HERB-1 is closely
111 related to the twentieth century US-1 genotype, suggesting that these two pandemic genotypes
112 may have emerged from a secondary metapopulation rather than from the species' Mexican
113 center of diversity.

114 **Results**

115 **Preservation of ancient DNA and genome statistics**

116 Nineteenth-century samples of potato and tomato leaves with *P. infestans* lesions were
117 obtained from the herbaria of the Botanische Staatssammlung München and the Kew Royal
118 Botanical Gardens (Table 1 and Figure 1). DNA was extracted under clean room conditions
119 and two genomic libraries were prepared from each sample for Illumina sequencing. The
120 preparations were expected to comprise *P. infestans* DNA, host DNA from potato or tomato
121 as well as DNA from microbes that had colonized either the living material at the time of its
122 collection, or the dried material during its storage in the herbaria.

123 The first set of libraries was used for verification of aDNA-like characteristics, and the
124 second set was used for production. In this second set we used a repair protocol that removes
125 aDNA-associated lesions, mainly characterized by cytosine deamination to uracil (U), which
126 is subsequently converted to and read as thymine (T) (Briggs et al., 2007; Briggs et al., 2010;
127 Brotherton et al., 2007; Hofreiter et al., 2001). The combination of uracil-DNA-glycosylase
128 (UDG) and endonuclease VIII, which removes uracil residues and repairs abasic sites, reduces
129 the overall per-base error rate to as low as one twentieth of unrepaired aDNA (Briggs et al.,
130 2010).

131 Ancient DNA fragments are typically shorter than 100 bp (Pääbo, 1989), and paired-
132 end reads of 100 bases each will therefore substantially overlap. Forward and reverse reads
133 from the unrepaired libraries (Table 2) were merged, requiring at least 11 base overlap.
134 Merging of short-insert libraries considerably decreases the error-rate and also generates
135 sequences that reflect the original molecule length (Kircher, 2012). The median length of
136 merged reads was in the range of ~50-85 bp (Figure 2a, b).

137 Merged sequences were mapped to the *P. infestans* T30-4 reference genome (Haas et
138 al., 2009). Deamination of C to U in aDNA is highest at the first base (Briggs et al., 2007),
139 and C-to-T was the predominant substitution at the 5'-end of molecules (Figure 2c, d). Based
140 on mapping against the reference genome, we estimated the fraction of *P. infestans* DNA in
141 the samples to be between 1 and 20% (Figure 2e). Most of the remaining reads could be
142 mapped to the reference genomes for potato and tomato
143 (Potato Genome Sequencing Consortium, 2011; The Tomato Genome Consortium, 2012).

144 In addition to 11 historic samples from Ireland, Great Britain, continental Europe and
145 North America (Figure 1 and Table 1), we shotgun sequenced 14 modern strains from
146 Europe, the Americas and Africa (Figure 1 and Table 1). These had been selected based on
147 preliminary mtDNA information to present a cross section of *P. infestans* diversity. Finally,
148 we sequenced two strains of *P. mirabilis*, P7722 and PIC99114, and a single strain of *P.*
149 *ipomoeae*, PIC99167. Both species are closely related to *P. infestans* and served as outgroups
150 (Kroon et al., 2004; Raffaele et al., 2010a). We considered genomes with mean-fold coverage
151 of at least 20 as high coverage; one historic, seven modern and both outgroup genomes
152 fulfilled this condition (Figure 3a). We identified single nucleotide polymorphisms (SNPs) in
153 each sample independently by comparison with the *P. infestans* reference T30-4 genome
154 (Figure 3b). Thresholds for calling homozygous and heterozygous SNPs were determined
155 from simulated data from high- and low-coverage genomes (Figure 3 – figure supplement 1).
156 We accepted SNPs from low-coverage genomes if the variants had also been called in a high-
157 coverage genome. Inverse cumulative coverage plots indicated how many high- or low-
158 coverage samples were needed to cover different fractions of SNPs (Figure 3c, d). A total of
159 4.5 million non-redundant SNPs were called. Eighty percent of all homozygous SNPs were
160 found in at least eight samples, and only twenty percent of all SNPs were found in fewer than
161 ten strains. Thus, the great majority of polymorphic sites were shared by several strains and
162 thus informative for phylogenetic analyses.

163

164 **A unique type I mtDNA haplotype in nineteenth century *P. infestans* strains**

165 We reconstructed the mtDNA genomes from historic and modern strains using an iterative
166 mapping assembler (Green et al., 2008) and estimated a phylogenetic tree from complete
167 mtDNA genomes, with one of the *P. mirabilis* mtDNA genomes as outgroup. Previous
168 studies have recognized four *P. infestans* mtDNA haplotype groups (Ia, Ib, IIa and IIb), based
169 on a small number of restriction fragment length polymorphisms (RFLPs) (Carter et al.,
170 1990). Surprisingly, a comparison of the complete mtDNA genomes revealed that the historic
171 samples did not fit into any of these groups, and instead formed an independent clade, called
172 HERB-1 from here on. Among the HERB-1 mtDNA genomes, there were very few
173 differences, with a mean pair-wise difference of only 0.2 bp, compared to 3.9 bp for the
174 modern haplotype I strains, and 9.0 bp for modern haplotype II strains. The origin of HERB-1
175 relative to haplotypes Ia and Ib could not be unequivocally resolved, and a polytomy was
176 inferred for these three groups or support for branches were low (Figure 4, and Figure 4 –
177 figure supplement 1).

178 The clonal lineage US-1, with the diagnostic mtDNA haplotype Ib, was the
179 predominant genotype throughout the world until about 1980 (Goodwin et al., 1994). The two
180 US-1 representatives in our material, DDR7602 (Germany) and LBUS5 (South Africa),
181 clustered together with the Ib reference genome and samples P6096 (Peru) and P1362
182 (Mexico) (Figure 4, and Figure 4 – figure supplement 1), even though these last two samples
183 had not been classified before as US-1 isolates. Although the US-1 genotype is closely related
184 to the herbarium strains, US-1 is not a derivative of HERB-1. Rather, HERB-1 and US-1 are
185 sister groups that share a common ancestor. There are three private substitutions that define
186 the US-1 clade, and two that define the HERB-1 clade. In agreement with the previous report
187 by Ristaino and colleagues (2001), all historic samples had a T at the position diagnostic for
188 haplotype Ib (Figure 4 – figure supplement 2), which distinguishes them from the US-1
189 lineage, which carries instead a C at this position. In contrast to the previous report (Ristaino
190 et al., 2001), we found no other sequence differences around this diagnostic site.

191

192 **Relationship between HERB-1 and modern strains and divergence times**

193 As the HERB-1 strains were sampled in the nineteenth century, their genomes should harbor
194 fewer substitutions compared to modern strains, which have continued to evolve for over a
195 hundred years. This can be exploited to directly calculate substitution rates and divergence
196 times using the sampling age as tip calibration in a Bayesian framework analysis. Shorter
197 evolutionary time usually translate into branch shortening in phylogenetic trees that include
198 both modern and ancient pathogen strains (Bos et al., 2011).. By calculating the nucleotide

199 distance to the outgroup P17777, all HERB-1 strains were found to show significantly fewer
200 mtDNA substitutions than modern strains with haplotype Ia or Ib ($p = 0.0003$). Sampling age
201 of the strain and the number of mtDNA substitutions were highly correlated ($r^2 = 0.8$; Figure
202 5).

203 Given the correlation between sample age and the number of mtDNA substitutions, a
204 multiple sequence alignment of 12 nearly complete modern and the 13 HERB-1 mtDNA
205 genomes was used as input for a Bayesian framework analysis using algorithms implemented
206 in the software package Beast (Drummond et al., 2012). The molecular clock hypothesis for
207 the modern strains could not be rejected at a 5% significance level ($p = 0.12$). Therefore, a
208 strict molecular clock and a birth-death tree prior (Stadler, 2010) were used for the Bayesian
209 framework analysis. Collection dates for all herbaria samples and the isolation dates for all
210 modern strains were used as tip calibration points, so that substitution rates per time interval
211 could be calculated (Table 1). Three Markov Chain Monte Carlo (MCMC) runs with 147
212 million iterations were carried out. Stability of the estimated prior and posterior probability
213 distributions (ESS values $>5,000$) and likelihood values (ESS values $>9,000$) were observed
214 in the trace files throughout the merged iterations using the software Tracer (Rambaut and
215 Drummond, 2007). From this procedure, we estimated the mtDNA substitution rate to be 2.4
216 $\times 10^{-6}$ per site and year ($1.5\text{-}3.3 \times 10^{-6}$, 95% HPD). This rate resulted in a mean divergence
217 time for *P. infestans* and *P. mirabilis* of 1,318 years ago (ya) (853-1,836 ya 95% HPD) and
218 for *P. infestans* type I and type II mtDNA haplotypes of 460 ya (300-643 ya 95% HPD). The
219 origin of the nineteenth century herbarium clade was estimated to around 182 ya (168-201 ya
220 95% HPD) (Figure 6, and Table 3).

221 To understand the evolutionary relationships between historical and modern strains in
222 more detail, we also compared their nuclear genomes. We built phylogenetic trees with high-
223 coverage genomes using maximum parsimony (Figure 7a), maximum likelihood (Figure 7b)
224 and neighbor-joining (Figure 7 – figure supplement 1) methods. We included in the analysis
225 heterozygous biallelic SNPs by random sampling an allele from each of them. In all cases,
226 the HERB-1 representative, M-0182896, formed a distinct, isolated clade that appeared as a
227 robust sister group to US-1 isolates DDR7602 and LBUS5. As a caveat, the random sampling
228 of SNPs at heterozygous positions will inflate bootstrap support. Nevertheless, a heat map
229 (Figure 7c) highlights that the two US-1 strains are both most closely related to HERB-1 and
230 the most distinct among modern strains. Phylogenetic analyses that included the low-coverage
231 genomes (Figure 7 – figure supplement 1) were consistent with a close relationship between
232 the HERB-1 and US-1 lineages.

233

234 **Ploidy increase in modern strains**

235 The independent diversification of the pandemic HERB-1 and US-1 lineages together with a
236 very recent common ancestor are consistent with both lineages having originated from the
237 same metapopulation. To test whether the global replacement of HERB-1 by US-1 in the
238 twentieth century was due to adaptive mutations, we searched for positively selected genes
239 using PAML (Yang, 2007). We did not find any evidence for genes or sites that had
240 experienced branch-specific positive selection in any of the lineages, only a mosaic pattern
241 with potentially positively selected genes shared across lineages. Alternative scenarios could
242 be that inactivating mutations were more important than non-synonymous substitutions, or
243 that higher overall diversity and re-assortment of beneficial gene variants by recombination
244 contributed to the success of US-1.

245 Genetic diversity can be increased by polyploidy, which has been reported in isolates
246 of *P. infestans* (e.g., Catal et al., 2010; Daggett et al., 1995), and which has major
247 evolutionary implications for asexual organisms. To estimate ploidy level in our specimens,
248 we investigated the distribution of read counts at biallelic SNPs for high-coverage genomes.
249 In a diploid species, the mean of read counts at heterozygous positions should have a single
250 mode at 0.5, while there should be two modes, 0.33 and 0.67, for triploid genomes, and three
251 modes, 0.25, 0.5 and 0.75 for tetraploid genomes. We compared the observed distributions of
252 read counts with computational simulations of diploid, triploid and tetraploid genomes. Based
253 on the shape and kurtosis of the distributions we concluded that the historic M-0182896
254 genome was apparently diploid. Of the modern genomes, only NL07434 and P17777 were
255 diploid, whereas the majority, including the two US-1 strains DDR7602 and LBUS5 as well
256 as P13527 and P13626 were triploid. One strain, 06_3928A, even seemed to be tetraploid
257 (Figure 8a, b, and Figure 8 – figure supplement 1). This conclusion was supported by
258 polyploid strains having evidence for triallelic polymorphism at many more sites than M-
259 0182896 (Figure 8c).

260 To further confirm the ploidy inferences, we classified 40,352 SNPs as derived or
261 ancestral based on information from the outgroup species *P. mirabilis* and *P. ipomoeae*. We
262 then compared the rate of homozygosity at derived alleles in M-0182896 and DDR7602. In
263 agreement with the ploidy difference, M-0182896 had more than twice as many derived
264 homozygous SNPs (8,375) than DDR7602 (3,440), regardless of annotation as synonymous,
265 non-synonymous and non-sense (Figure 9a, b).

266

267 **Effector genes**

268 *Phytophthora infestans* secretes a large repertoire of effector proteins, some of which are
269 recognized by plant immune receptors encoded by *R* genes (Haas et al., 2009; Vleeshouwers
270 et al., 2011). These *R* genes occur in wild potato (*Solanum*) species mostly originating from
271 the pathogen center of diversity in Mexico, and have been introduced by breeding into
272 cultivated potato since the beginning of the twentieth century (Hawkes, 1990). The analysis of
273 effector gene sequences in HERB-1 strains should reveal the effector repertoire prior to its
274 disruption by the selective forces imposed by resistance gene breeding. Given that nineteenth
275 century potato cultivars in North America and Europe were fully susceptible to late blight, we
276 presume that they did not yet contain resistance genes that are effective against HERB-1.
277 Conversely, the first *R* genes for *P. infestans* resistance, introduced into cultivated potato only
278 after the dates for our HERB-1 samples, should be effective against HERB-1 strains, which
279 are predicted to carry matching avirulence effector genes. The *R* genes include in particular
280 *R1* to *R4* from *Solanum demissum* (Hawkes, 1990).

281 To date, ten avirulence effector genes, recognized by ten matching *Solanum R* genes,
282 have been described in *P. infestans* (Vleeshouwers et al., 2011). We first estimated the
283 presence/absence profiles of these effector genes based on the fraction of gene length that was
284 covered by reads ('breadth of coverage') in each high-coverage genome, and by merged reads
285 from low-coverage genomes (Table 4). We deduced the amino acid sequences of these ten
286 effectors using both alignments of reads to the reference genome and *de novo* assemblies. All
287 examined avirulence effector genes except *Avr3b* were present as full-length and intact coding
288 sequences in the historic samples (Table 4), without any frame shift or nonsense mutations.
289 The HERB-1 alleles of *Avr1*, *Avr2*, *Avr3a* and *Avr4* were shared with those of the US-1 strain
290 DDR7602 (Table 5 and source file 1). In conclusion, the *Avr1*, *Avr2*, *Avr3a* and *Avr4* alleles
291 of HERB-1 are intact, presumably functional copies that are identical to ones that can be
292 recognized by the matching *R* genes *R1*, *R2*, *R3a* and *R4* (Armstrong et al., 2005; Gilroy et
293 al., 2011; van Poppel et al., 2008; Vleeshouwers et al., 2011). This is consistent with the
294 expectation that the HERB-1 genotype must have been avirulent on the first potato cultivars
295 that acquired late blight resistance.

296 We examined in more detail *Avr3a*, which is recognized by *Solanum demissum R3a*.
297 The two major *Avr3a* alleles encode secreted proteins that differ in two amino acids in their
298 effector domains: AVR3a^{KI} and AVR3a^{EM} (Figure 10a, and Figure 10 – figure supplement 1).
299 Only the AVR3a^{KI} type triggers signaling by the resistance protein R3a (Armstrong et al.,
300 2005). The *R3a* gene was introduced into modern potato from *S. demissum* at the beginning of

301 the twentieth century, providing modern potato with resistance against the *P. infestans* strains
302 prevalent at the time (Gebhardt and Valkonen, 2001; Hawkes, 1990; Huang et al., 2005).
303 Strains homozygous for *Avr3a*^{EM}, which avoids *R3a*-mediated detection of the pathogen,
304 appeared later; US-1 isolates lack *Avr3a*^{EM} (Armstrong et al., 2005). Examination of *Avr3a*
305 SNPs in the historic samples only revealed the AVR3a^{KI} allele, whereas both alleles were
306 present in modern samples (Figure 10b). To confirm that the potato hosts of the historic
307 strains lacked the ability to recognize AVR3a^{KI}, we assembled *de novo* short reads from the
308 historic samples and aligned them against the *R3a* sequence from modern potato (Huang et
309 al., 2005). As expected, we only found *R3* homologs that were distinct in sequence from *R3a*
310 (Figure 10c).

311 The absence of the *Avr3b* effector gene in HERB-1 could be viewed as puzzling, given
312 that the *S. demissum* *R3* locus was one of the first to be bred into potato. However, *R3b*, the
313 matching *R* gene of *Avr3b*, is within 0.4 cM of *R3a* in the complex *R3* locus (Li et al., 2011).
314 Based on the absence of an *Avr3b* gene in HERB-1, we conclude that initial introgression of
315 the *R3* locus from *S. demissum* was based on the resistance phenotype conferred by the *R3a*
316 gene. The *R3* phenotype scored during the initial introgression must have been the recognition
317 of *Avr3a* by *R3a*, and the presence of *R3b* must have been irrelevant until *P. infestans* strains
318 carrying *Avr3b* emerged.

319 Discussion

320 To characterize the *P. infestans* strain(s) that triggered the Irish potato famine, we have
321 sequenced several mtDNA and nuclear genomes of nineteenth century *P. infestans* strains.
322 Because we wanted to interpret our findings in the context of extant genetic diversity, we
323 investigated several modern strains as well. We could reconstruct the phylogenetic
324 relationship between historic and modern strains using dozens of variants in complete
325 mtDNA genomes, and millions of SNPs in the nuclear genomes, compared to previous work
326 that had to rely on three mtDNA SNPs (May and Ristaino, 2004; Ristaino et al., 2001). The
327 topologies of mtDNA and nuclear phylogenies were very similar, with the nuclear genomes
328 yielding additional insights into differences in heterozygosity, ploidy levels and effector gene
329 complement between historic and modern strains. Contrary to previous inferences (May and
330 Ristaino, 2004; Ristaino et al., 2001), the nineteenth century strains are closely related to the
331 modern US-1 lineage, but are characterized by a single, distinct mtDNA haplotype, HERB-1.

332 Finally, from estimates of the divergence times of the different lineages, we were able to
333 associate key events in *P. infestans* evolution with historic records of human migration and
334 late blight spread.

335

336 **Relationship between historical and modern strains**

337 Historic strains from different geographic locations all carried a mtDNA haplotype, HERB-1,
338 that had not been recognized before (Figure 4). Although collected over a period of 50 years,
339 the strains were distinguished from each other by few nuclear SNPs, indicating that the
340 nineteenth century outbreak was a true pandemic of a rapidly spreading clonal genotype. That
341 HERB-1 has so far not been found in any modern strain may point to its extinction after the
342 nineteenth century pandemic, possibly associated with the onset of resistance gene breeding
343 in the twentieth century. We cannot, however, exclude that HERB-1 still infects some
344 localized, genetically unimproved host populations, since we have explored only a fraction of
345 current *P. infestans* genetic diversity. With the diagnostic variants we have discovered, one
346 can now probe modern populations to determine whether or not HERB-1 still persists
347 somewhere.

348 Historic pathogen samples are molecular fossils that can be used as tip calibration
349 points to estimate major divergence events in the evolution of a pathogen (Bos et al., 2011).
350 Using the collection dates of the herbarium samples and isolation dates of the modern *P.*
351 *infestans* strains, we estimated that type I and type II mtDNA haplotypes diverged close to the
352 beginning of the sixteenth century (Figure 6, and Table 3). This coincides with the first
353 contact between Americans and Europeans in Mexico, which potentially fuelled *P. infestans*
354 population migration and expansion outside its center of diversity. This major event in human
355 history might thus have been responsible for wider dissemination of the *P. infestans* pathogen
356 in the New World, several centuries before its introduction to Europe. In addition, the
357 divergence estimates allowed us to date the split between *P. mirabilis* and *P. infestans* about
358 1,300 ya. Even though this was firmly during the period of pre-Columbian civilization, what
359 led to their relatively recent speciation remains unknown.

360 To test the congruence of mtDNA and nuclear phylogenies, we reconstructed
361 phylogenies with over four million nuclear SNPs from high-quality genomes (Figure 7). This
362 confirmed the historic sample M-0182896 as a sister group to US-1 strains, a conclusion that
363 was supported by a broader analysis that included the low-coverage historic samples (Figure 7
364 – figure supplement 1). The private SNPs shared by the HERB-1 lineage ruled out that US-1
365 isolates are, as previously proposed (Goodwin et al., 1994), direct descendants of the historic

366 strains. Nevertheless, US-1 is more closely related to the historic strains than to the modern
367 strains that have come to dominate the global population in the past two decades.

368 We therefore propose a revision of the previous scenario, which posited that a single
369 *P. infestans* lineage migrated around 1842 or 1843 from Mexico to North America, from
370 where it was soon transferred to Europe, followed by global dissemination and persistence for
371 over hundred years (Goodwin et al., 1994). Our data make it likely that by the late 1970s,
372 direct descendants of HERB-1 had either become rare or extinct. On the other hand, the close
373 relationship between HERB-1 and US-1 suggests that the US-1 lineage originated from a
374 similar source as HERB-1, with our divergence estimates indicating that the two lineages
375 separated only in the early nineteenth century. Given the much greater genetic diversity at the
376 species' likely origin in Mexico, it seems unlikely that HERB-1 and US-1 spread
377 independently from this region. An alternative scenario is that a small *P. infestans*
378 metapopulation was established at the periphery of its center of origin, or even outside
379 Mexico, possibly in North America, some time before the first global *P. infestans* pandemic.
380 The first lineage to spread from there was HERB-1, which persisted globally for at least half a
381 century. Subsequently, the US-1 lineage expanded and spread, replacing HERB-1 (Figure 11).

382

383 **Genetic and genomic differences between historic and modern strains**

384 Host *R* genes that confer resistance to historic *P. infestans* strains, such as *R3a*, were bred into
385 cultivated potato *Solanum tuberosum* from the wild species *S. demissum* at the beginning of
386 the twentieth century, years after our youngest historic sample had been collected in 1896. In
387 agreement with the products of these *R* genes being able to recognize HERB-1 effectors,
388 HERB-1 strains seem to have only the *Avr3a^{KI}* allele, which interacts with the product of the
389 *R* gene *R3a* to trigger a host immune response (Armstrong et al., 2005; Huang et al., 2005).
390 Moreover, *de novo* assembly of potato DNA did not provide evidence for the presence of *R3a*
391 in the herbarium hosts, consistent with the narrative of potato breeding (Figure 10c) (Hawkes,
392 1990). While it is uncertain when HERB-1 was displaced by the US-1 lineage, the US-1
393 lineage also carries only the *Avr3a^{KI}* allele (Armstrong et al., 2005). The origin of the
394 *Avr3a^{EM}* allele that emerged to high frequency after the breeding of *R3a* into cultivated
395 potatoes remains unclear.

396 A major genomic difference between the HERB-1 and US-1 lineages is the shift in
397 ploidy, from diploid to triploid and even tetraploid (Figure 8, and figure 8 – figure supplement
398 1). Polyploidization could have provided an opportunity for US-1 isolates to enhance allelic
399 diversity in the absence of frequent sexual reproduction, and could thus have contributed to

400 their global success. Asexual reproduction leads to an increase of deleterious mutation in the
401 population due to a lack of meiotic recombination (Felsenstein, 1974). Therefore, if the major
402 selection pressure that led to the replacement of HERB-1 by US-1 was the introduction of
403 resistance gene breeding, greater variation at effector genes in polyploid US-1 strains could
404 have contributed to the replacement of HERB-1 soon after *R* genes from *S. demissum* and
405 other wild species had been introduced into modern potato germplasm.

406

407 **Conclusions**

408 We present the first genome-wide analyses of historic plant pathogen strains. The aDNA in
409 the herbarium samples, which were about 150 years old, was remarkably well conserved,
410 much better than most examples of aDNA from animals and humans, and only comparable
411 with permafrost samples (Miller et al., 2008; Rasmussen et al., 2010).

412 Our analyses not only highlight how knowledge of the genetics and geographic
413 distribution of modern strains is insufficient to correctly infer the source of historic epidemics
414 (Goodwin et al., 1994), but they also reveal the shortcomings of inferences that are based on a
415 very small number of genetic markers in historic strains (May and Ristaino, 2004; Ristaino et
416 al., 2001). With our much richer dataset, we could demonstrate that the late blight outbreaks
417 during the nineteenth century were a pandemic caused by a single *P. infestans* lineage, but
418 that this lineage was not the direct ancestor of the one that had come to dominate the global *P.*
419 *infestans* population during much of the twentieth century. Infected plant specimens stored in
420 herbaria around the world are thus a largely untapped source to learn about events that
421 affected millions of people during our recent history.

422 **Material and methods**

423 **Herbarium sampling**

424 Plant specimens were sent to the Senckenberg Museum in Frankfurt am Main by the
425 Botanische Staatssammlung München and the Kew Royal Botanical Gardens, where potato
426 and tomato leaves with lesions indicative of *P. infestans* infection were sampled, retrieving
427 both the lesions and healthy surrounding tissue. Sampling was carried out under sterile
428 conditions in a laboratory with no prior exposure to *P. infestans*. Samples were subsequently
429 sent to the Palaeogenetics laboratory at the University of Tübingen.

430

431 **DNA extraction and sequencing library preparation**

432 Preamplification steps of historic samples were performed in clean room facilities with no
433 prior exposure to *P. infestans* DNA. Samples were extracted following the protocol of
434 (Kistler, 2012), using 380 to 500 µg of each sample. Tissue was crushed with mortar and
435 pestle, 1.2 ml extraction buffer (1% SDS, 10 mM Tris pH 8.0, 5 mM NaCl, 50 mM DTT, 0.4
436 mg/mL proteinase K, 10 mM EDTA, 2.5 mM *N*-phenacylthiazolium bromide) was added, and
437 samples were incubated over night at 37°C with constant agitation. A modified protocol with
438 the Qiagen Plant DNEasy Mini kit was then used to purify the extracted DNA.

439 Two independent Illumina sequencing libraries were created for each DNA extract. In
440 the first library, C-to-T damage caused by deamination of cytosines (Hofreiter et al., 2001)
441 was not repaired. Twenty µl of each DNA extract, extraction blank control and water library
442 blank control were converted into sequencing libraries as described (Meyer and Kircher,
443 2010) with modifications for aDNA (Meyer et al., 2012). To avoid potential sequencing
444 artifacts caused by DNA damage, a second library was made from, 30 µl of each DNA
445 extract, extraction blank control and water library blank control, and treated with uracil-DNA
446 glycosylase (UDG) and Endonuclease VIII before conversion into sequencing libraries
447 (Briggs et al., 2010). Each library received sample-specific double indices after preparation
448 via amplification with two ‘index’ PCR primers (Meyer et al., 2012). Indexed libraries were
449 individually amplified in 100 µl reactions containing 5 µl library template, 2 units of
450 AccuPrime Pfx DNA polymerase (Invitrogen), 1 unit of 10×PCR Mix and 0.3 µM primers
451 spanning the index sequences of the libraries. The following thermal profile was used: 2-min
452 initial denaturation at 95°C, 2 or 3 cycles consisting of 15 sec denaturation at 95°C, a 30-sec
453 annealing at 60°C and a 2-min elongation at 68°C, and a 5-min final elongation at 68°C.
454 Amplified products were purified and quantified on an Agilent 2100 Bioanalyzer DNA 1000
455 chip.

456 DNA extracts of the modern *P. infestans* samples P17721, P10650, P6096, P11633,
457 P10127, P9464, P12204 and P13626 and *P. mirabilis* P7722 were obtained from the World
458 Phytophthora and Oomycete Genetic Resource Collection, fragmented to 300 bp using a S220
459 Covaris instrument according to the manufacturers’ protocol (Duty cycle 10%, intensity 4,
460 cycles per burst 200, time (sec) 120), and converted into sequencing libraries following the
461 above steps as described for the historic samples without UDG treatment (Kircher, 2012;
462 Meyer et al., 2012). For *P. mirabilis* PIC99114 and *P. ipomoeae* PIC99167, genomic DNA
463 used before (Cooke et al., 2012; Raffaele et al., 2010b) was converted into Illumina

464 sequencing libraries. Genomic DNA from the other modern strains was isolated as described
465 (Cooke et al., 2012).

466 Libraries were sequenced on Illumina GAIIx, HiSeq 2000 or MiSeq instruments,
467 (Table 2). To estimate the fraction of *P. infestans* aDNA in the herbarium samples, we
468 performed pilot sequencing. Once the samples with the highest amount of *P. infestans* were
469 identified, production runs were carried out on an Illumina HiSeq 2000 instrument. For *P.*
470 *infestans* 06_3928A analysis, we used publicly available short reads (ENA ERP002420).

471

472 **Read mapping and SNP calling**

473 Reads for the herbarium samples were de-indexed as described (Kircher, 2012). Forward and
474 reverse reads were merged after adapter trimming, requiring at least 11 nucleotides overlap
475 (Burbano et al., 2010). Only fragments that that allowed merging of reads were used in
476 subsequent analyses. Merged reads were mapped to the *P. infestans* T30-4 reference genome
477 (Haas et al., 2009) with BWA, allowing two gaps and without seeding (Li and Durbin, 2009).
478 PCR duplicates were identified based on read start and end alignment coordinates. For each
479 cluster of duplicates a consensus sequence was calculated as described (Kircher, 2012). Only
480 reads with a Phred-like mapping quality score of at least 30 were used further. Alignments
481 were converted to BAM files (Li et al., 2009). For modern strains, single reads were mapped
482 in a similar manner, and subsequent processing was performed as described (Cooke et al.,
483 2012).

484 SNPs in the herbarium samples were called by independently comparing each strain
485 with the *P. infestans* T30-4 genome. Raw allele counts for each position were obtained using
486 pileup from SAMtools (Li et al., 2009). To decide the cutoffs for SNP calling we resorted to
487 simulations. Reads from two 50-fold and 3-fold coverage genomes were simulated using the
488 pIRS software (Hu et al., 2012), with empirical base-calling and GC%-depth profiles trained
489 on five modern *P. infestans* genomes (P13527, P13626, 06_3928A, NL07434 and P17777).
490 Based on the simulated data we called both homo and heterozygous SNPs employing
491 different cutoffs for SNP concordance (Figure 3 – figure supplement 1). Genotypes calls were
492 classified as high quality if coverage was at least 10. We also considered low-quality SNPs, if
493 a high-quality SNP call had been made in a different strain, using specific coverage cutoffs
494 for rescuing low-quality SNPs (Figure 3 – figure supplement 1). We calculated sensitivity
495 and accuracy of SNP calls for different combination of cutoffs and selected the following
496 criteria:

- 497 • Minimum coverage of 10 for high quality calls.

- 498 • Concordance \geq 80% for homozygous SNPs.
- 499 • Concordance between 20-80% for heterozygous SNPs.
- 500 • Minimum coverage of 3 to rescue low-quality SNPs.

501 We called synonymous, nonsynonymous and nonsense polymorphisms employing
502 snpEff (Cingolani et al., 2012).

503

504 **Mitochondrial DNA (mtDNA) assembly and phylogenetic analyses**

505 Fragments that could be aligned to any of the four reference haplotypes (Ia, IIa, Ib and IIb)
506 were used to assemble mtDNA genomes. For each strain four different assemblies (one for
507 each reference haplotype) were built using an iterative mapping assembly program (Burbano
508 et al., 2010; Green et al., 2008). Only positions with coverage of at least 3 were included in
509 the assemblies. The four assemblies were aligned using Kalign (Lassmann and Sonnhammer,
510 2005) with default parameters, and a consensus assembly was generated based on the
511 alignment.

512 The 1.8 kb insertion present in haplotype II was not considered for phylogenetic
513 reconstruction. The mtDNA phylogeny was built using a maximum parsimony and a
514 maximum likelihood tree using MEGA5 (Tamura et al., 2011). For both, positions with less
515 than 90% site coverage were eliminated. There were a total of 24,560 positions in the final
516 dataset, compared to the multiple sequence alignment length (37,762 bp). For the maximum
517 likelihood reconstruction we used the Hasegawa-Kishino-Yano (HKY) model assuming that a
518 certain fraction of sites are evolutionarily invariable. The model was selected using MEGA5
519 (Tamura et al., 2011).

520

521 **Nuclear genome phylogenetic analyses**

522 We reconstructed the nuclear phylogeny for the high-coverage samples alone and for all
523 samples together independently, using maximum parsimony and maximum likelihood
524 approaches. We built the neighbor-joining trees based on a genetic distance matrix calculated
525 from both homo- and heterozygous SNPs (Xu et al., 2012). For the high-coverage genomes
526 we used only the SNPs positions with complete information in all samples. For the low-
527 coverage genomes we used homo- and heterozygous SNPs, and allowing for missing data. So
528 that we could include heterozygous SNPs in the analysis, we randomly sampled one allele at
529 each site. The maximum parsimony trees were calculated with 100 replicates in MEGA5
530 using the Close-Neighbor-Interchange algorithm with search level 0, in which the initial trees

531 were obtained with the random addition of sequences (10 replicates). All positions with less
532 than 95% site coverage were eliminated (Tamura et al., 2011). For the high-coverage
533 genomes-only analysis, all positions with less than 85% site coverage were eliminated. For
534 the all-sample analysis the threshold was lowered to 80%. Maximum likelihood trees were
535 built using RaxML 7.0.4 with 100 replicates using the rapid bootstrap algorithm (Stamatakis,
536 2006).

537

538 **Effector analyses**

539 To address presence and absence polymorphisms of effectors, we used a previously published
540 pipeline (Raffaele et al., 2010a). We calculated the fraction of each gene that was covered by
541 reads ('breadth of coverage') for each strain. We regarded zero breadth of coverage as
542 absence of the gene. For herbarium and modern samples with genome-wide coverage depth
543 less than 20x, we merged BAM files from each strain into a single BAM file, and used this to
544 estimate breadth of coverage.

545 We also tested for presence/absence polymorphisms of RXLR effector genes between
546 herbarium samples and modern strains using *de novo* assembly of short reads. First, we
547 extracted 140 bp fragments from M-0182896 merged reads, and assembled these with
548 SOAPdenovo v1.05 (Luo et al., 2012). We aligned the six-frame translation of resulting
549 contigs to a non-redundant protein database using blastx (Altschul et al., 1990). Most contigs
550 matched proteins from either potato, *Solanum tuberosum*, or to microbial species *P. infestans*,
551 *Pantoea vagans* and *Pseudomonas* sp. To focus on *P. infestans*, we aligned fragments that
552 were at least 140 bp to the genomes of *P. infestans*, *S. tuberosum*, *P. vagans*, *P. syringae* pv.
553 *syringae*, and *P. fluorescens* with blastn. We extracted fragments that aligned the *P. infestans*
554 genomic regions encoding RXLR effector genes, but over at most 90 bp. These and
555 unmapped fragments were *de novo* assembled with SOAPdenovo v1.05. A *k*-mer size of 67
556 was deemed optimal, because it resulted in the highest coverage of *Avr1*, *Avr2* and *Avr3a*, and
557 resulted in the largest number of RXLR proteins with TBLASTN hits (Figure 10 – figure
558 supplement 1). We obtained partial sequences of *Avr4* and *Avrblb1*. We visually evaluated
559 BWA alignments of M-0182896 in the *Avr4* and *Avrblb1* genomic regions and identified T30-
560 4 sequences uncovered by alignments using Integrative Genomics Viewer (Robinson et al.,
561 2011). We then identified T30-4 genomic regions with at least 99% similarity to these
562 uncovered regions. In BWA, if reads match several genomic regions, one genomic location is
563 randomly chosen as default (Li and Durbin, 2009). Thus, it is possible that BWA alignment
564 distributes reads coming from the same gene across several, closely related genes in the target

565 genome. We assembled such reads that mapped to closely related sequences in the reference
566 genome together with the partial sequences of *Avr4* and *Avrblb1* using Geneious® Pro 5.6.3
567 to obtain full-length sequences of these *Avr* genes.

568

569 **Selection tests**

570 Homozygous SNPs from modern *P. infestans* strains EC3527, EC3626, NL07434, 06_3928A,
571 DDR7602, LBUS5, P17777 and the historic strain M-0182896 were used for selection tests.
572 Gene sequences were converted into amino acid sequences using EMBOSS tools (Rice et al.,
573 2000), and Pla2Nal v14 (Suyama et al., 2006) was used to convert protein alignments to
574 codon alignments. The codeml module of PAML package v4.6 (Yang, 2007) was used for
575 positive selection studies with site models M7 (parameters NSsites = 7, fix_omega = 0,
576 omega = 2 and kappa = 3) and M8 (NSsites = 8, fix_omega = 0, omega = 2 and kappa = 3). A
577 5% level of significance was established with Likelihood ratio test. Genes were considered to
578 be under positive selection if at least one site was found to be under selection with a Bayes
579 Empirical Bayes confidence >95%.

580

581 **Ploidy analyses**

582 To estimate ploidy levels, we assessed the distributions of read counts at biallelic SNPs. For
583 diploid species, the mean frequency of reads for each allele at non-homozygous sites is 1/2,
584 while we expect two modes for triploid genomes, at 1/3 and 2/3, and four modes for tetraploid
585 genomes, at 1/4, 1/2 and 3/4 (Figure 8a). We simulated genomes with different ploidy levels
586 using pIRS (Hu et al., 2012), based on two strains, *P. infestans* T30-4 and EC3527. The SNPs
587 used for the construction of two simulated chromosomes were determined with SAMtools
588 v0.1.8 mpileup and bcftools v0.1.17 (Li et al., 2009). For the diploid genome, we simulated
589 10x coverage reads for each of two different chromosomes. For the triploid genome, we
590 merged simulated 5x and 15x coverage reads from two different chromosomes. For the
591 tetraploid genome, we merged simulated 10x coverage reads from two different chromosomes
592 (Figure 8b). Next, we aligned the simulated reads to the *P. infestans* T30-4 reference genome
593 with BWA and called heterozygous SNPs under the following criteria: minimum coverage of
594 10 for high-quality calls, and concordance between 20-80% for heterozygous SNPs. Since
595 tetraploid species are considered to be a mixtures of two ratio, we mixed SNPs from the 20x
596 coverage diploid reads and the 20x coverage tetraploid reads in following ratios: 0:100, 10:90,
597 20:80, 30:70, 40:60, 50:50, 60:40, 70:30, 80:20, 90:10 and 100:0. Finally, we estimated
598 frequency of reads assigning each allele at each SNP position. Based on shapes, standard

599 deviation, skewedness and kurtosis of the observed distributions and comparison with the
600 simulated distributions, we classified the tested *P. infestans* genomes as diploid, triploid and
601 tetraploid.

602

603 **Substitution rates and divergence times for *P. infestans***

604 In order to test whether we can detect a temporal signal in the ancient *P. infestans* mtDNA
605 sequences compared to modern strains, i.e. shorter branches in the ancient strains compared to
606 the modern ones, we calculated the nucleotide distance as the number of substitutions
607 between HERB-1, haplotype Ia and haplotype Ib mtDNA genomes to the outgroup P17777.
608 The analysis involved 19 nucleotide sequences. All positions with less than 90% site coverage
609 were eliminated, resulting in 34,174 informative positions. The samples were subsequently
610 grouped into ancient and modern strains. The ancient and modern nucleotide distances were
611 significantly different (Mann-Whitney U-test, $p = 0.0003$). We furthermore correlated the
612 nucleotide distance of HERB-1, haplotype Ia and haplotype Ib mtDNA genomes to the
613 outgroup P17777 with the tip age of each sample.

614 To estimate divergence times of *P. infestans* strains, substitution rates were calculated
615 in a Bayesian framework analysis using the software package BEAST 1.7.5 (Drummond et
616 al., 2012). A multiple sequence alignment that included all 12 nearly complete modern *P.*
617 *infestans* mtDNA sequences plus all 13 herbaria samples was used as input. In order to test if
618 the mtDNAs evolved clock like a likelihood ratio test was performed in MEGA5 (Tamura et
619 al., 2011) by comparing the maximum likelihood (ML) value for the given topology using
620 only the modern strains with and without the molecular clock constraints. The null hypothesis
621 of equal evolutionary rate throughout the tree was not rejected at a 5% significance level ($P =$
622 0.115). All positions containing gaps and missing data were eliminated resulting in a total of
623 22,591 positions in the final dataset.

624 As a result a strict molecular clock and the HKY sequence evolution model were used
625 for the Bayesian framework. For the tree prior, five different models were tested including
626 four coalescence models: constant size, expansion growth, exponential growth, logistic
627 growth and a epidemiology birth-death model (Stadler, 2010). For each tree prior, three
628 MCMC runs were carried out with 10,000,000 iterations each and subsequently merged using
629 LogCombiner 1.7.5 from the BEAST package. Resulting ESS values and overall posterior
630 likelihoods were compared using the software Tracer (Rambaut and Drummond, 2007). The
631 birth-death model gave the highest ESS values and posterior likelihood and was therefore
632 chosen for the subsequent dating analysis. The collection dates for all herbaria samples as

633 well as the isolation dates for all modern strains were used as tip calibration points (Table 1).
634 Three MCMC runs were carried out with 50,000,000 iterations each, sampling every 10,000
635 steps. The first 1,000,000 iterations were discarded as burn-in resulting in a total of
636 147,000,000 iterations.

637 **Bibliography**

- 638 Altschul, S.F., Gish, W., Miller, W., Myers, E.W., and Lipman, D.J. (1990). Basic local
639 alignment search tool. *J. Mol. Biol.* *215*, 403-410.
- 640 Armstrong, M.R., Whisson, S.C., Pritchard, L., Bos, J.I., Venter, E., Avrova, A.O., Rehmany,
641 A.P., Bohme, U., Brooks, K., Cherevach, I., et al. (2005). An ancestral oomycete locus
642 contains late blight avirulence gene *Avr3a*, encoding a protein that is recognized in the host
643 cytoplasm. *Proc. Natl. Acad. Sci. USA* *102*, 7766-7771.
- 644 Bos, K.I., Schuenemann, V.J., Golding, G.B., Burbano, H.A., Waglechner, N., Coombes,
645 B.K., McPhee, J.B., DeWitte, S.N., Meyer, M., Schmedes, S., et al. (2011). A draft
646 genome of *Yersinia pestis* from victims of the Black Death. *Nature* *478*, 506-510.
- 647 Bos, K.I., Stevens, P., Nieselt, K., Poinar, H.N., Dewitte, S.N., and Krause, J. (2012). *Yersinia*
648 *pestis*: new evidence for an old infection. *PLoS ONE* *7*, e49803.
- 649 Bourke, P.M.A. (1964). Emergence of potato blight, 1843-46. *Nature* *203*, 805-808.
- 650 Briggs, A.W., Stenzel, U., Johnson, P.L., Green, R.E., Kelso, J., Prüfer, K., Meyer, M.,
651 Krause, J., Ronan, M.T., Lachmann, M., et al. (2007). Patterns of damage in genomic
652 DNA sequences from a Neandertal. *Proc. Natl. Acad. Sci. USA* *104*, 14616-14621.
- 653 Briggs, A.W., Stenzel, U., Meyer, M., Krause, J., Kircher, M., and Pääbo, S. (2010). Removal
654 of deaminated cytosines and detection of in vivo methylation in ancient DNA. *Nucleic*
655 *Acids Res.* *38*, e87.
- 656 Brotherton, P., Endicott, P., Sanchez, J.J., Beaumont, M., Barnett, R., Austin, J., and Cooper,
657 A. (2007). Novel high-resolution characterization of ancient DNA reveals C > U-type base
658 modification events as the sole cause of post mortem miscoding lesions. *Nucleic Acids*
659 *Res.* *35*, 5717-5728.
- 660 Burbano, H.A., Hodges, E., Green, R.E., Briggs, A.W., Krause, J., Meyer, M., Good, J.M.,
661 Maricic, T., Johnson, P.L., Xuan, Z., et al. (2010). Targeted investigation of the Neandertal
662 genome by array-based sequence capture. *Science* *328*, 723-725.

663 Carter, D.A., Archer, S.A., Buck, K.W., Shaw, D.S., and Shattock, R.C. (1990). Restriction
664 fragment length polymorphisms of mitochondrial DNA of *Phytophthora infestans*. Mycol.
665 Res. 94, 1123-1128.

666 Catal, M., King, L., Tumbalam, P., Wiriyajitsomboon, P., Kirk, W.W., and Adams, G.C.
667 (2010). Heterokaryotic nuclear conditions and a heterogeneous nuclear population are
668 observed by flow cytometry in *Phytophthora infestans*. Cytometry. Part A : the journal of
669 the International Society for Analytical Cytology 77, 769-775.

670 Cingolani, P., Platts, A., Wang le, L., Coon, M., Nguyen, T., Wang, L., Land, S.J., Lu, X.,
671 and Ruden, D.M. (2012). A program for annotating and predicting the effects of single
672 nucleotide polymorphisms, SnpEff: SNPs in the genome of Drosophila melanogaster strain
673 *w¹¹¹⁸; iso-2; iso-3*. Fly 6, 80-92.

674 Cooke, D.E., Cano, L.M., Raffaele, S., Bain, R.A., Cooke, L.R., Etherington, G.J., Deahl,
675 K.L., Farrer, R.A., Gilroy, E.M., Goss, E.M., et al. (2012). Genome analyses of an
676 aggressive and invasive lineage of the Irish potato famine pathogen. PLoS Pathog. 8,
677 e1002940.

678 Daggett, S.S., Knighton, J.E., and Therrien, C.D. (1995). Polyploidy among isolates of
679 *Phytophthora infestans* from Eastern Germany. J. Phytopathol. 143, 419-422.

680 de Bary, H.A. (1876). Researches into the nature of the potato fungus, *Phytophthora*
681 *infestans*. J. Roy. Agric. Soc. Engl. Ser. 2 12, 239-269.

682 Drummond, A.J., Suchard, M.A., Xie, D., and Rambaut, A. (2012). Bayesian phylogenetics
683 with BEAUti and the BEAST 1.7. Mol. Biol. Evol. 29, 1969-1973.

684 Felsenstein, J. (1974). The evolutionary advantage of recombination. Genetics 78, 737-756.

685 Fisher, M.C., Henk, D.A., Briggs, C.J., Brownstein, J.S., Madoff, L.C., McCraw, S.L., and
686 Gurr, S.J. (2012). Emerging fungal threats to animal, plant and ecosystem health. Nature
687 484, 186-194.

688 Flier, W.G., Grunwald, N.J., Kroon, L.P., Sturbaum, A.K., van den Bosch, T.B., Garay-
689 Serrano, E., Lozoya-Saldana, H., Fry, W.E., and Turkensteen, L.J. (2003). The population
690 structure of *Phytophthora infestans* from the Toluca Valley of Central Mexico suggests
691 genetic differentiation between populations from cultivated potato and wild *Solanum*
692 species. Phytopathology 93, 382-390.

693 Fry, W. (2008). *Phytophthora infestans*: the plant (and R gene) destroyer. Mol. Plant Pathol.
694 9, 385-402.

695 Fry, W., Grünwald, N., D, C., A, M., G, F., and K, C. (2009). Population genetics and
696 population diversity of *Phytophthora infestans*. In Oomycete Genetics and Genomics:

697 Diversity, Interactions, and Research Tools, K. Lamour, and S. Kamoun, eds. (Hoboken,
698 NJ, Wiley-Blackwell), pp. 139-164.

699 Fry, W.E., Goodwin, S.B., Matuszak, J.M., Spielman, L.J., Milgroom, M.G., and Drenth, A.
700 (1992). Population genetics and intercontinental migrations of *Phytophthora infestans*.
701 *Annu. Rev. Phytopathol.* *30*, 107-129.

702 Gavino, P.D., and Fry, W.E. (2002). Diversity in and evidence for selection on the
703 mitochondrial genome of *Phytophthora infestans*. *Mycologia* *94*, 781-793.

704 Gebhardt, C., and Valkonen, J.P. (2001). Organization of genes controlling disease resistance
705 in the potato genome. *Annu. Rev. Phytopathol.* *39*, 79-102.

706 Gilroy, E.M., Breen, S., Whisson, S.C., Squires, J., Hein, I., Kaczmarek, M., Turnbull, D.,
707 Boevink, P.C., Lokossou, A., Cano, L.M., et al. (2011). Presence/absence, differential
708 expression and sequence polymorphisms between *PiAVR2* and *PiAVR2-like* in
709 *Phytophthora infestans* determine virulence on *R2* plants. *New Phytol.* *191*, 763-776.

710 Goodwin, S.B., Cohen, B.A., and Fry, W.E. (1994). Panglobal distribution of a single clonal
711 lineage of the Irish potato famine fungus. *Proc. Natl. Acad. Sci. USA* *91*, 11591-11595.

712 Green, R.E., Malaspina, A.S., Krause, J., Briggs, A.W., Johnson, P.L., Uhler, C., Meyer, M.,
713 Good, J.M., Maricic, T., Stenzel, U., et al. (2008). A complete Neandertal mitochondrial
714 genome sequence determined by high-throughput sequencing. *Cell* *134*, 416-426.

715 Grünwald, N.J., and Flier, W.G. (2005). The biology of *Phytophthora infestans* at its center of
716 origin. *Annu. Rev. Phytopathol.* *43*, 171-190.

717 Haas, B.J., Kamoun, S., Zody, M.C., Jiang, R.H., Handsaker, R.E., Cano, L.M., Grabherr, M.,
718 Kodira, C.D., Raffaele, S., Torto-Alalibo, T., et al. (2009). Genome sequence and analysis
719 of the Irish potato famine pathogen *Phytophthora infestans*. *Nature* *461*, 393-398.

720 Hawkes, J.G. (1990). *The Potato: Evolution, Biodiversity and Genetic Resources*
721 (Washington, D.C., Smithsonian Institution Press).

722 Hofreiter, M., Jaenicke, V., Serre, D., Haeseler Av, A., and Pääbo, S. (2001). DNA sequences
723 from multiple amplifications reveal artifacts induced by cytosine deamination in ancient
724 DNA. *Nucleic Acids Res.* *29*, 4793-4799.

725 Hu, X., Yuan, J., Shi, Y., Lu, J., Liu, B., Li, Z., Chen, Y., Mu, D., Zhang, H., Li, N., et al.
726 (2012). pIRS: Profile-based Illumina pair-end reads simulator. *Bioinformatics* *28*, 1533-
727 1535.

728 Huang, S., van der Vossen, E.A., Kuang, H., Vleeshouwers, V.G., Zhang, N., Borm, T.J., van
729 Eck, H.J., Baker, B., Jacobsen, E., and Visser, R.G. (2005). Comparative genomics
730 enabled the isolation of the *R3a* late blight resistance gene in potato. *Plant J.* *42*, 251-261.

731 Kamoun, S., Hraber, P., Sobral, B., Nuss, D., and Govers, F. (1999). Initial assessment of
732 gene diversity for the oomycete pathogen *Phytophthora infestans* based on expressed
733 sequences. *Fungal Genet. Biol.* *28*, 94-106.

734 Kircher, M. (2012). Analysis of high-throughput ancient DNA sequencing data. *Methods*
735 *Mol. Biol.* *840*, 197-228.

736 Kistler, L. (2012). Ancient DNA extraction from plants. *Methods Mol. Biol.* *840*, 71-79.

737 Kroon, L.P., Bakker, F.T., van den Bosch, G.B., Bonants, P.J., and Flier, W.G. (2004).
738 Phylogenetic analysis of *Phytophthora* species based on mitochondrial and nuclear DNA
739 sequences. *Fungal Genet. Biol.* *41*, 766-782.

740 Lassmann, T., and Sonnhammer, E.L. (2005). Kalign--an accurate and fast multiple sequence
741 alignment algorithm. *BMC Bioinformatics* *6*, 298.

742 Li, G., Huang, S., Guo, X., Li, Y., Yang, Y., Guo, Z., Kuang, H., Rietman, H., Bergervoet,
743 M., Vleeshouwers, V.G., et al. (2011). Cloning and characterization of *R3b*; members of
744 the *R3* superfamily of late blight resistance genes show sequence and functional
745 divergence. *Mol. Plant Microbe Interact.* *24*, 1132-1142.

746 Li, H., and Durbin, R. (2009). Fast and accurate short read alignment with Burrows-Wheeler
747 transform. *Bioinformatics* *25*, 1754-1760.

748 Li, H., Handsaker, B., Wysoker, A., Fennell, T., Ruan, J., Homer, N., Marth, G., Abecasis, G.,
749 and Durbin, R. (2009). The Sequence Alignment/Map format and SAMtools.
750 *Bioinformatics* *25*, 2078-2079.

751 Luo, R., Liu, B., Xie, Y., Li, Z., Huang, W., Yuan, J., He, G., Chen, Y., Pan, Q., Liu, Y., et al.
752 (2012). SOAPdenovo2: an empirically improved memory-efficient short-read de novo
753 assembler. *GigaScience* *1*, 18.

754 May, K.J., and Ristaino, J.B. (2004). Identity of the mtDNA haplotype(s) of *Phytophthora*
755 *infestans* in historical specimens from the Irish potato famine. *Mycol. Res.* *108*, 471-479.

756 Meyer, M., and Kircher, M. (2010). Illumina sequencing library preparation for highly
757 multiplexed target capture and sequencing. *Cold Spring Harb. Protoc.* *2010*, pdb prot5448.

758 Meyer, M., Kircher, M., Gansauge, M.T., Li, H., Racimo, F., Mallick, S., Schraiber, J.G., Jay,
759 F., Prufer, K., de Filippo, C., et al. (2012). A high-coverage genome sequence from an
760 archaic Denisovan individual. *Science* *338*, 222-226.

761 Miller, W., Drautz, D.I., Ratan, A., Pusey, B., Qi, J., Lesk, A.M., Tomsho, L.P., Packard,
762 M.D., Zhao, F., Sher, A., et al. (2008). Sequencing the nuclear genome of the extinct
763 woolly mammoth. *Nature* *456*, 387-390.

764 Pääbo, S. (1989). Ancient DNA: extraction, characterization, molecular cloning, and
765 enzymatic amplification. *Proc. Natl. Acad. Sci. USA* 86, 1939-1943.

766 Pääbo, S., Poinar, H., Serre, D., Jaenicke-Despres, V., Hebler, J., Rohland, N., Kuch, M.,
767 Krause, J., Vigilant, L., and Hofreiter, M. (2004). Genetic analyses from ancient DNA.
768 *Annu. Rev. Genet.* 38, 645-679.

769 Perez, W.G., Gamboa, J.S., Falcon, Y.V., Coca, M., Raymundo, R.M., and Nelson, R.J.
770 (2001). Genetic structure of peruvian populations of *Phytophthora infestans*.
771 *Phytopathology* 91, 956-965.

772 Potato Genome Sequencing Consortium (2011). Genome sequence and analysis of the tuber
773 crop potato. *Nature* 475, 189-195.

774 Raffaele, S., Farrer, R.A., Cano, L.M., Studholme, D.J., MacLean, D., Thines, M., Jiang,
775 R.H., Zody, M.C., Kunjeti, S.G., Donofrio, N.M., et al. (2010a). Genome evolution
776 following host jumps in the Irish potato famine pathogen lineage. *Science* 330, 1540-1543.

777 Raffaele, S., Win, J., Cano, L.M., and Kamoun, S. (2010b). Analyses of genome architecture
778 and gene expression reveal novel candidate virulence factors in the secretome of
779 *Phytophthora infestans*. *BMC Genomics* 11, 637.

780 Rambaut, A., and Drummond, A. (2007). Tracer v1.4. <http://beast.bio.ed.ac.uk/Tracer>

781 Rasmussen, M., Li, Y., Lindgreen, S., Pedersen, J.S., Albrechtsen, A., Moltke, I., Metspalu,
782 M., Metspalu, E., Kivisild, T., Gupta, R., et al. (2010). Ancient human genome sequence of
783 an extinct Palaeo-Eskimo. *Nature* 463, 757-762.

784 Reader, J. (2009). *Potato: A History of the Propitious Esculent* (New Haven, Yale University
785 Press).

786 Rice, P., Longden, I., and Bleasby, A. (2000). EMBOSS: the European Molecular Biology
787 Open Software Suite. *Trends Genet.* 16, 276-277.

788 Ristaino, J.B., Groves, C.T., and Parra, G.R. (2001). PCR amplification of the Irish potato
789 famine pathogen from historic specimens. *Nature* 411, 695-697.

790 Robinson, J.T., Thorvaldsdottir, H., Winckler, W., Guttman, M., Lander, E.S., Getz, G., and
791 Mesirov, J.P. (2011). Integrative genomics viewer. *Nat. Biotechnol.* 29, 24-26.

792 Stadler, T. (2010). Sampling-through-time in birth-death trees. *J Theor Biol* 267, 396-404.

793 Stamatakis, A. (2006). RAxML-VI-HPC: maximum likelihood-based phylogenetic analyses
794 with thousands of taxa and mixed models. *Bioinformatics* 22, 2688-2690.

795 Suyama, M., Torrents, D., and Bork, P. (2006). PAL2NAL: robust conversion of protein
796 sequence alignments into the corresponding codon alignments. *Nucleic Acids Res.* 34,
797 W609-612.

798 Tamura, K., Peterson, D., Peterson, N., Stecher, G., Nei, M., and Kumar, S. (2011). MEGA5:
799 molecular evolutionary genetics analysis using maximum likelihood, evolutionary
800 distance, and maximum parsimony methods. *Mol. Biol. Evol.* 28, 2731-2739.

801 The Tomato Genome Consortium (2012). The tomato genome sequence provides insights into
802 fleshy fruit evolution. *Nature* 485, 635-641.

803 Tooley, P.W., Fry, W.E., and Gonzalez, M.J.V. (1985). Isozyme characterization of sexual
804 and asexual *Phytophthora infestans* populations. *J. Hered.* 76, 431-435.

805 Turner, R.S. (2005). After the famine: Plant pathology, *Phytophthora infestans*, and the late
806 blight of potatoes, 1845-1960. *Hist. Stud. Phys. Biol. Sci.* 35, 341-370.

807 van Poppel, P.M., Guo, J., van de Vondervoort, P.J., Jung, M.W., Birch, P.R., Whisson, S.C.,
808 and Govers, F. (2008). The *Phytophthora infestans* avirulence gene *Avr4* encodes an
809 RXLR-dEER effector. *Mol. Plant Microbe Interact.* 21, 1460-1470.

810 Vleeshouwers, V.G., Raffaele, S., Vossen, J.H., Champouret, N., Oliva, R., Segretin, M.E.,
811 Rietman, H., Cano, L.M., Lokossou, A., Kessel, G., et al. (2011). Understanding and
812 exploiting late blight resistance in the age of effectors. *Annu. Rev. Phytopathol.* 49, 507-
813 531.

814 Xu, X., Liu, X., Ge, S., Jensen, J.D., Hu, F., Li, X., Dong, Y., Gutenkunst, R.N., Fang, L.,
815 Huang, L., et al. (2012). Resequencing 50 accessions of cultivated and wild rice yields
816 markers for identifying agronomically important genes. *Nat. Biotechnol.* 30, 105-111.

817 Yang, Z. (2007). PAML 4: phylogenetic analysis by maximum likelihood. *Mol. Biol. Evol.*
818 24, 1586-1591.

819

820 **Acknowledgments**

821 We are indebted to Bryn Dentinger, curator of the herbarium of the Kew Royal Botanical
822 Gardens, and to Dagmar Triebel, curator of the herbarium of the Botanische Staatssammlung
823 München, for providing the historic specimens used in this study. We are grateful to Mike
824 Coffey for discussion of strain selection for genome analyses and providing genomic DNA
825 preparations, Tahir Ali for help with phylogenetic tests, Jodie Pike for sequencing support,
826 and Mike Coffey, David Cooke, Geert Kessel, Adele McLeod, Ricardo Oliva and Vivianne
827 Vleeshouwers for *Phytophthora* strains. We thank Axel Künstner, Dan Koenig, Jorge

828 Quintana and Ignacio Rubio-Somoza for discussion on data analysis and Eunyoung Chae and
829 Rebecca Schwab for comments on the manuscript.

830

831

832

833

835 **Table 1.** Provenance of *P. infestans* samples.

	ID	Country of origin	Collection year	Host species	Reference*
Herbarium samples	KM177500	England	1845	<i>Solanum tuberosum</i>	1
	KM177513	Ireland	1846	<i>Solanum tuberosum</i>	1
	KM177502	England	1846	<i>Solanum tuberosum</i>	1
	KM177497	England	1846	<i>Solanum tuberosum</i>	1
	KM177514	Ireland	1847	<i>Solanum tuberosum</i>	1
	KM177548	England	1847	<i>Solanum tuberosum</i>	1
	KM177507	England	1856	<i>Petunia hybrida</i>	1
	M-0182898	Germany	Before 1863	<i>Solanum tuberosum</i>	2
	KM177509	England	1865	<i>Solanum tuberosum</i>	1
	M-0182900	Germany	1873	<i>Solanum lycopersicum</i>	2
	M-0182907	Germany	1875	<i>Solanum tuberosum</i>	1
	KM177517	Wales	1875	<i>Solanum tuberosum</i>	1
	M-0182897	USA	1876	<i>Solanum lycopersicum</i>	2
	M-0182906	Germany	1877	<i>Solanum tuberosum</i>	2
	M-0182896	Germany	1877	<i>Solanum tuberosum</i>	2
	M-0182904	Austria	1879	<i>Solanum tuberosum</i>	2
	M-0182903	Canada	1896	<i>Solanum tuberosum</i>	2
	KM177512	England	NA	<i>Solanum tuberosum</i>	1
Modern samples	06_3928A	England	2006	<i>Solanum tuberosum</i>	3
	DDR7602	Germany	1976	<i>Solanum tuberosum</i>	4
	P1362	Mexico	1979	<i>Solanum tuberosum</i>	5
	P6096	Peru	1984	<i>Solanum tuberosum</i>	5
	P7722 (<i>P. mirabilis</i>)	USA	1992	<i>Solanum lycopersicum</i>	5
	P9464	USA	1996	<i>Solanum tuberosum</i>	5
	P12204	Scotland	1996	<i>Solanum tuberosum</i>	5
	P13527	Ecuador	2002	<i>Solanum andreamum</i>	5
	P10127	USA	2002	<i>Solanum lycopersicum</i>	5
	P13626	Ecuador	2003	<i>Solanum tuberosum</i>	5
	P10650	Mexico	2004	<i>Solanum tuberosum</i>	5
	LBUS5	South Africa	2005	<i>Petunia hybrida</i>	6
	P11633	Hungary	2005	<i>Solanum lycopersicum</i>	5
	NL07434	Netherlands	2007	<i>Solanum tuberosum</i>	3
	P17777	USA	2009	<i>Solanum lycopersicum</i>	5
	P17721	USA	2009	<i>Solanum tuberosum</i>	5

837

838

839

840

841

*1, Kew Royal Botanical Gardens; 2, Botanische Staatssammlung München; 3, (Cooke et al., 2012); 4, (Kamoun et al., 1999); 5, World Oomycete Genetic Resource Collection at UC Riverside, CA; 6, Dr. Adele McLeod, Univ. of Stellenbosch, South Africa

842 **Table 2.** Sequencing strategy.

ID	Instrument and read type	Sequencing center	Coverage
M-0182896	HiSeq 2000 (2x101 bp)	MPI	High
M-0182897	HiSeq 2000 (2x101 bp)	MPI	Low ¹
M-0182898	HiSeq 2000 (2x101 bp)	MPI	Low
M-0182900	HiSeq 2000 (2x101 bp)	MPI	Low ²
M-0182903	HiSeq 2000 (2x101 bp)	MPI	Low
M-0182904	HiSeq 2000 (2x101 bp)	MPI	Low ¹
M-0182906	HiSeq 2000 (2x101 bp)	MPI	Low ²
M-0182907	HiSeq 2000 (2x101 bp)	MPI	Low
KM177497	MiSeq (2x150 bp)	MPI	Low
KM177500	MiSeq (2x150 bp)	MPI	Low ¹
KM177502A	MiSeq (2x150 bp)	MPI	Low ¹
KM177507	MiSeq (2x150 bp)	MPI	Low ¹
KM177509	MiSeq (2x150 bp) & HiSeq 2000 (2x101 bp)	MPI	Low
KM177512	MiSeq (2x150 bp) & HiSeq 2000 (2x101 bp)	MPI	Low
KM177513	MiSeq (2x150 bp) & HiSeq 2000 (2x101 bp)	MPI	Low
KM177514	MiSeq (2x150 bp) & HiSeq 2000 (2x101 bp)	MPI	Low
KM177517	MiSeq (2x150 bp) & HiSeq 2000 (2x101 bp)	MPI	Low
KM177548	MiSeq (2x150 bp) & HiSeq 2000 (2x101 bp)	MPI	Low
06_3928A	GAIIX (2x76 bp)	TSL	High
DDR7602	GAIIX (2x76 bp)	TSL	High
LBUS5	GAIIX (2x76 bp)	TSL	High
NL07434	GAIIX (2x76 bp)	TSL	High
P10127	HiSeq 2000 (2x101 bp)	MPI	Low
P10650	HiSeq 2000 (2x101 bp)	MPI	Low
P12204	HiSeq 2000 (2x101 bp)	MPI	Low
P13527	GAIIX (2x76 bp)	TSL	High
P1362	HiSeq 2000 (2x101 bp)	MPI	Low
P13626	GAIIX (2x76 bp)	TSL	High
P11633	HiSeq 2000 (2x101 bp)	MPI	Low
P17721	HiSeq 2000 (2x101 bp)	MPI	Low
P17777	GAIIX (2x76 bp)	TSL	High
P6096	HiSeq 2000 (2x101 bp)	MPI	Low
P7722	HiSeq 2000 (2x101 bp)	MPI	Low
P9464	HiSeq 2000 (2x101 bp)	MPI	Low ¹
PIC99114	GAIIX (2x76 bp)	TSL	High
PIC99167	GAIIX (2x76 bp)	TSL	High

843

844 ¹Samples not included in any analysis due to extremely low coverage

845 ²Samples used only in mtDNA analysis.

846 **Table 3.** Inferred time to most recent common ancestor (TMRCA) for different splits in the mtDNA tree.

Node	TMRCA (ya)		
	Best estimate	Lower 2.5%	Upper 2.5%
I/HERB-1, II	460	300	643
Ia/Ib, HERB-1	234	187	290
HERB-1 strains	182	168	201
IIa, IIb	142	78	214

847

848

849

850

851

852

853

854

855

856

857

858 **Table 4.** Presence or absence of avirulence effector genes in historic and modern samples, expressed as percentages of effector genes covered by
 859 reads. Sequences and polymorphisms are shown in Table 5 and Table 5 – Source data 1.

<i>Avr</i> gene	<i>R</i> gene	HERB-1 [†]	US-1	20 th century non-US-1						Outgroups	
				EC3527	EC3626	P17777	06_3928A	NL07434	Merged	Pm PIC99114	Pip PIC99167
<i>Avr1</i>	<i>R1</i>	100	100	100	0	100	0	0	100	98	100
<i>Avr2</i>	<i>R2</i>	100	100	100	100	100	81	100	77	97	100
<i>Avr3a</i>	<i>R3a</i>	100	100	100	100	100	100	100	100	0	28
<i>Avr3b</i>	<i>R3b</i>	0	0	0	0	100	0	0	100	100	100
<i>Avr4</i>	<i>R4</i>	100	100	100	100	95	89	100	99	85	92
<i>Avrblb1</i>	<i>Rpi-blb1</i>	100	100	100	100	100	100	100	100	0	0
<i>Avrblb2</i>	<i>Rpi-blb2</i>	100	100	100	100	92	100	100	89	88	0
<i>Avrvnt1</i>	<i>Rpi-vnt1</i>	100	100	100	100	100	100	100	100	100	100
<i>AvrSmira1</i>	<i>Rpi-Smira1</i>	100	100	100	100	100	100	100	100	97	100
<i>AvrSmira2</i>	<i>Rpi-Smira2</i>	100	100	100	100	100	100	100	100	100	0

860

861 † Same sequences obtained for M-0182896 and merged sequences.

862 * Same sequences obtained for DDR7602 and LBUS5.

863

864

865

866

867 **Table 5.** Amino acid differences in the avirulence effectors AVR1, AVR2, AVR3a and
868 AVR4 encoded by the T30-4 reference genome, HERB-1 and DDR7602 (US-1). IDs in
869 parentheses refer to gene models in reference genome. Full-length sequences of deduced
870 amino acid sequences of HERB-1 AVR1, AVR2, AVR3a and AVR4 are provided in Table5 –
871 Source data 1.
872

Position	Substitution			Note
	T30-4	HERB1	DDR7602	
AVR1 (PITG_16663)				
80	T	T	T, S	HERB-1 polymorphisms shared with T30-4 and DDR7602.
142	I	I, T	T	
154	V	V, A	A	
185	I	I	I, V	
AVR2 (PITG_22870)				
31	N	K	K	HERB-1 identical to DDR7602.
AVR3a (PITG_14371)				
19	S	C	C	HERB-1 identical to DDR7602; both correspond to AVR3a ^{KI} isoform.
80	E	K	K	
103	M	I	I	
139	M	L	L	
AVR4 (PITG_07387)				
19	T	T, I	T	HERB-1 polymorphisms shared with T30-4 and DDR7602.
139	L	S	L, S	
221	L	V	L, V	
271	V	F	V, F	

873
874
875
876
877
878
879

Table 5 – Source data 1. Full-length sequences of deduced amino acid sequences of HERB-1 AVR1, AVR2, AVR3a and AVR4.

880

Figure 1. Countries of origin of samples used in whole-genome, mtDNA genome or both analyses. Red indicates number of historic and blue of modern samples. More information on the samples is given in Table 1 and Table 2.

883

Figure 2. Ancient DNA-like characteristic of historic samples. (A) Lengths of merged reads from historic sample M-0182898. **(B)** Mean lengths of merged reads from historic samples. **(C)** Nucleotide mis-incorporation in reads from the historic sample M-0182898. **(D)** Deamination at first 5' end base in historic samples. **(E)** Percentage of merged reads that mapped to the *P. infestans* reference genome.

889

890 **Figure 3. Coverage and SNP statistics.** (A) Mean nuclear genome coverage from historic
891 (red) and modern (blue) samples. (B) Homo- and heterozygous SNPs in each sample. (C)
892 Inverse cumulative coverage for all homozygous SNPs across all samples. (D) Same as (C)
893 for homo- and heterozygous SNPs.

894

895 **Figure 3 – figure supplement 1. Accuracy and sensitivity of SNP calling at different**
896 **cutoffs for SNP concordance based on 3- and 50-fold coverage of simulated data.** Rescue
897 cov. – minimum coverage required to accept SNP calls in low-coverage genomes based on
898 these SNPs having been found in high-coverage genomes. The cutoffs enclosed in orange
899 rectangles were used for the final analysis.

900

901 **Figure 4. Maximum-parsimony phylogenetic tree of complete mtDNA genomes.** Sites
902 with less than 90% information were not considered, leaving 24,560 sites in the final dataset.
903 Numbers at branches indicate bootstrap support (100 replicates), and scale indicates changes.

904

905 **Figure 4 – figure supplement 1. Maximum-likelihood phylogenetic tree of complete**
906 **mtDNA genomes.** Sites with less than 90% information were not considered, leaving 24,560
907 sites in the final dataset. Numbers at branches indicate bootstrap support (100 replicates).

908

909 **Figure 4 – figure supplement 2. mtDNA sequences around diagnostic *MspI* restriction**
910 **site (grey) for reference haplotype modern strains (blue) and historic strains (red).** The
911 *MspI* (CCGG) restriction site is only present in the Ib haplotype; all other strains have a C-to-
912 T substitution (CTGG).

913

914 **Figure 5. Correlation between nucleotide distance of mtDNA genomes of HERB-**
915 **1/haplotype Ia/haplotype Ib clade to the outgroup P17777 and sample age in calendar**
916 **years before present.**

917

918 **Figure 6. Divergence estimates of mtDNA genomes.** Bayesian consensus tree from 147,000
919 inferred trees. Posterior probability support above 50% is shown next to each node. Blue
920 horizontal bars represent the 95% HPD interval for the node height. Light yellow bars
921 indicate major historical events discussed in the text. See Figure 5 – Table 3 for detailed
922 estimates at the four main nodes in *P. infestans*.

923

924 **Figure 7. Phylogenetic trees of high-coverage nuclear genomes using both homozygous**
925 **and heterozygous SNPs. (A)** Maximum-parsimony tree, considering only sites with at least
926 95% information, leaving 4,498,351 sites in the final dataset. Numbers at branches indicate
927 bootstrap support (100 replicates), and scale indicates genetic distance. **(B)** Maximum-
928 likelihood tree. **(C)** Heat map of genetic differentiation (color scale indicates SNP
929 differences). US-1 strains DDR7062 and LBUS5 have the genomes sequences closest to M-
930 0182896 (asterisks). The two US-1 isolates in turn are outliers compared to all other modern
931 strains (highlighted by a gray box).

932

933 **Figure 7 – figure supplement 1. Phylogenetic trees of high- and low-coverage nuclear**
934 **genomes. (A)** Neighbor-joining tree of high-coverage genomes using 4,595,012 homo- and
935 heterozygous SNPs. Numbers at branches indicate bootstrap support (100 replicates), and
936 scale indicates genetic distance. **(B)** Neighbor-joining tree of high- and low-coverage
937 genomes using 2,101,039 homozygous and heterozygous SNPs. Numbers at branches indicate
938 bootstrap support above 50, from 100 replicates) Scale indicates genetic distance. **(C)**
939 Maximum parsimony tree of high- and low-coverage genomes using 315,394 SNPs
940 homozygous and heterozygous SNPs (using only sites with at least 80% information).

941

942 **Figure 8. Ploidy analysis. (A)** Diagram of expected read frequencies of reads at biallelic
943 SNPs for diploid, triploid and tetraploid genomes. **(B)** Reference read frequency at biallelic
944 SNPs in gene dense regions (GDRs) for the historic sample M-0182896, two modern samples,
945 and simulated diploid, triploid and tetraploid genomes. The simulated tetraploid genome is
946 assumed to have 20 % of pattern 1 and 80 % of pattern 3 shown in (A). The shape and
947 kurtosis of the observed distributions are similar to the corresponding simulated ones. **(C)**
948 Polymorphic positions with more than one allele in the GDR.

949

950 **Figure 8 – figure supplement 1. Reference read frequency at biallelic SNPs in gene dense**
951 **regions (GDRs) for five modern high-coverage samples.**

952

953 **Figure 9. Read allele frequencies of historic genome M-0182896 and US-1 isolate**
954 **DDR7602.** Alleles were classified as ancestral or derived using outgroup species *P. mirabilis*
955 and *P. ipomoeae*. There were 40,532 segregating sites. **(A)** Distributions of derived alleles at

956 sites segregating between M-0182896 and DDR7602. **(B)** Annotation of the different site
957 classes.

958

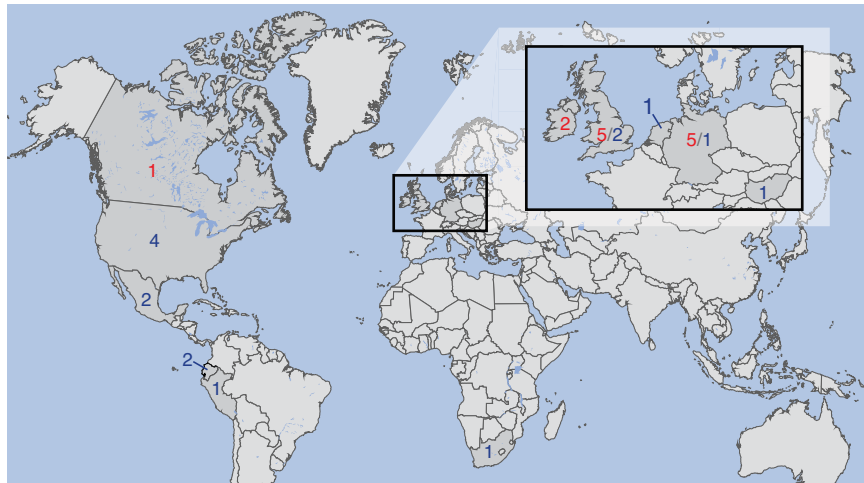
959 **Figure 10. The effector gene *Avr3a* and its cognate resistance gene *R3a*.** (A) Diagram of
960 AVR3A effector protein. (B) Frequency of *Avr3a* alleles in historic and modern *P. infestans*
961 strains. (C) Neighbor-joining tree of *R3a* homologs from potato, based on 0.67 kb partial
962 nucleotide sequences of *S. tuberosum* *R3a* (blue, accession number AY849382.1) and
963 homologs (dark grey) in GenBank, and *de novo* assembled contigs from M-0182896 (red).
964 Numbers at branches indicate bootstrap support with 500 replicates. Scale indicates changes.

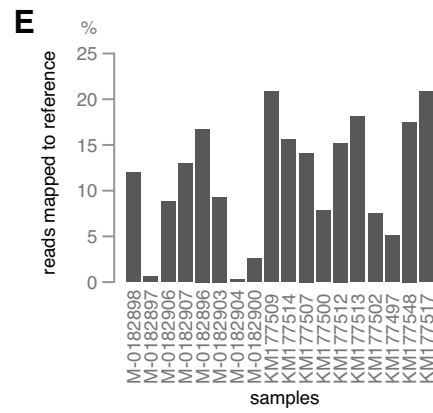
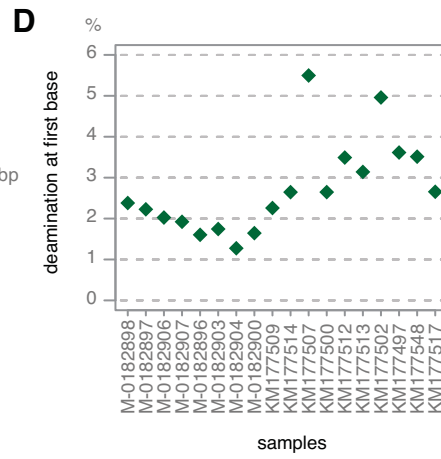
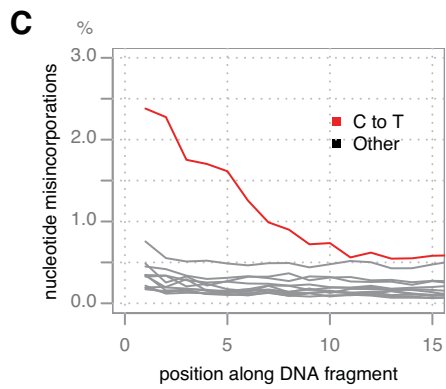
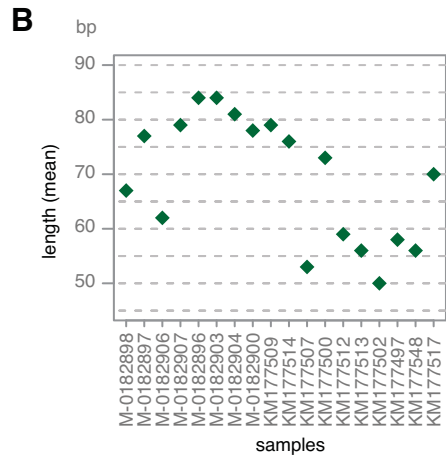
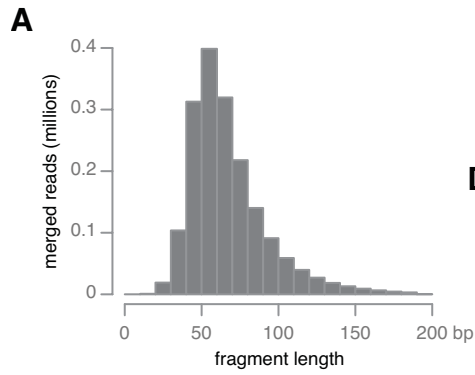
965

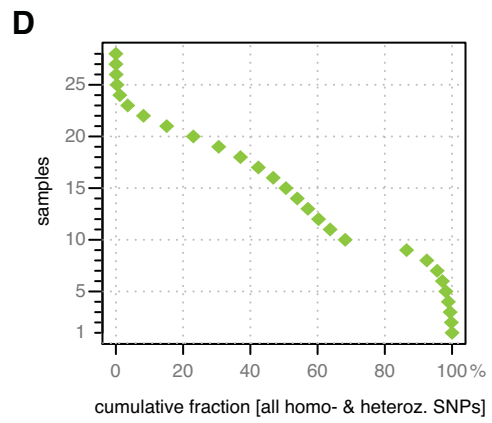
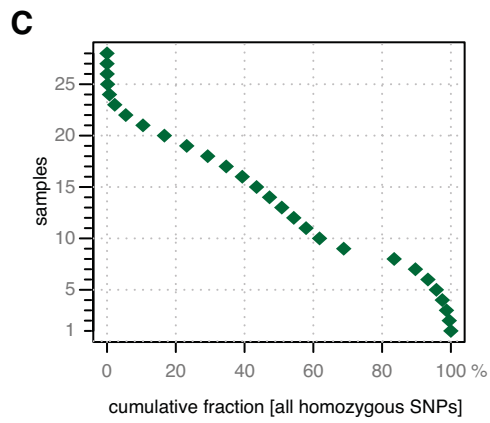
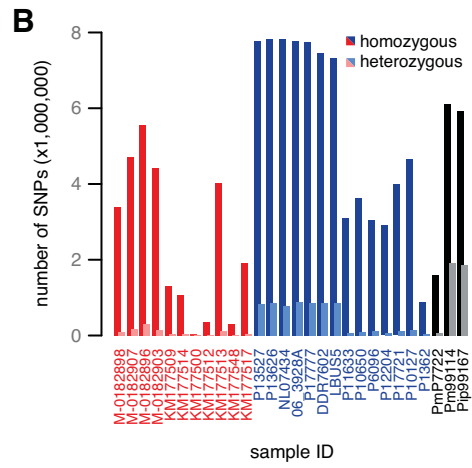
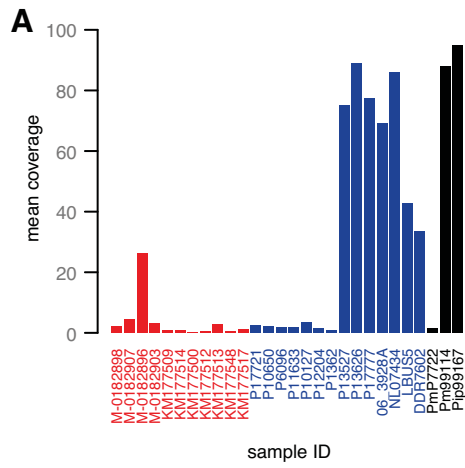
966 **Figure 10 – figure supplement 1. Summary of *de novo* assembly of RXLR effector genes.**
967 TBLASTN query was performed with 549 RXLR proteins as a query and contigs as a
968 database. When the High-scoring Segment Pair (HSP) and matched amino acids both covered
969 $\geq 99\%$ of the query length, we recorded a hit. Results with the optimal *k*-mer size are
970 highlighted.

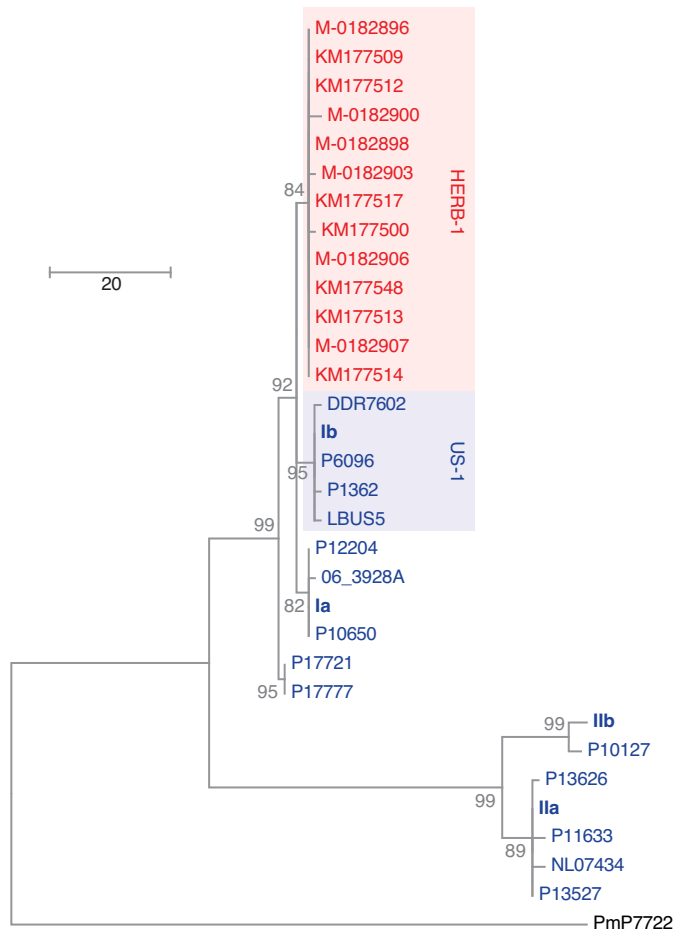
971

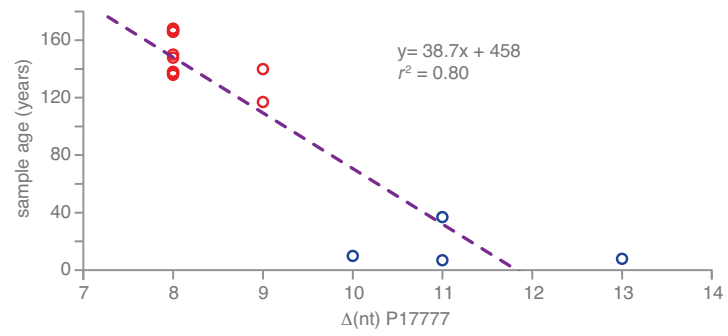
972 **Figure 11. Suggested paths of migration and diversification of *P. infestans* lineages**
973 **HERB-1 and US-1.** The location of the metapopulation that gave rise to HERB-1 and US-1
974 remains uncertain; here it is proposed to have been in North America.

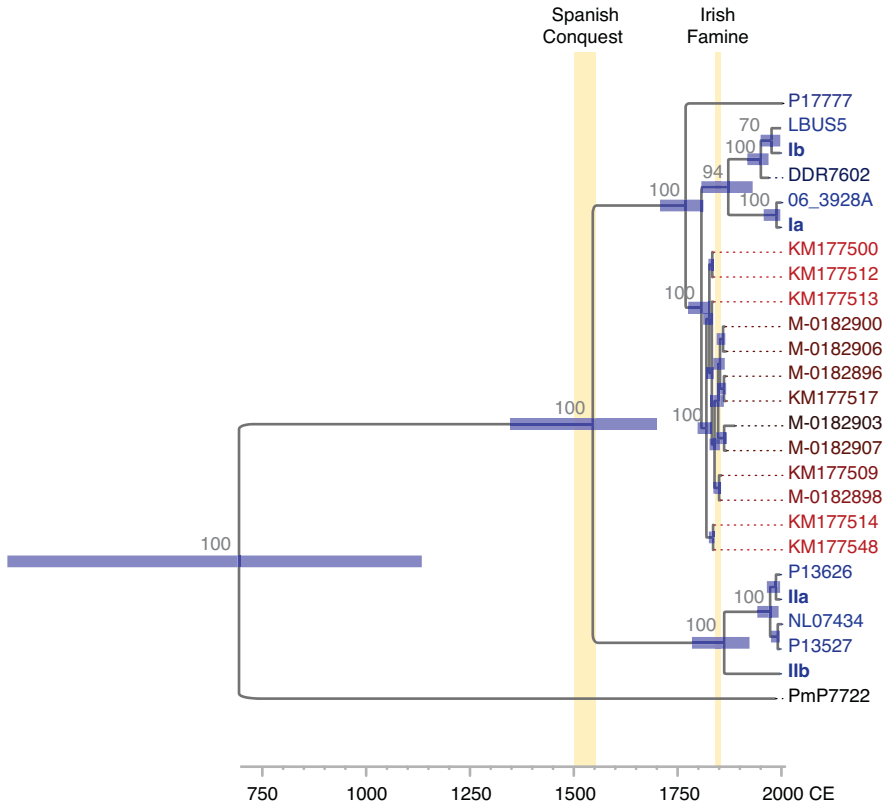


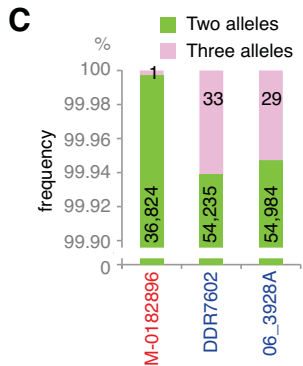
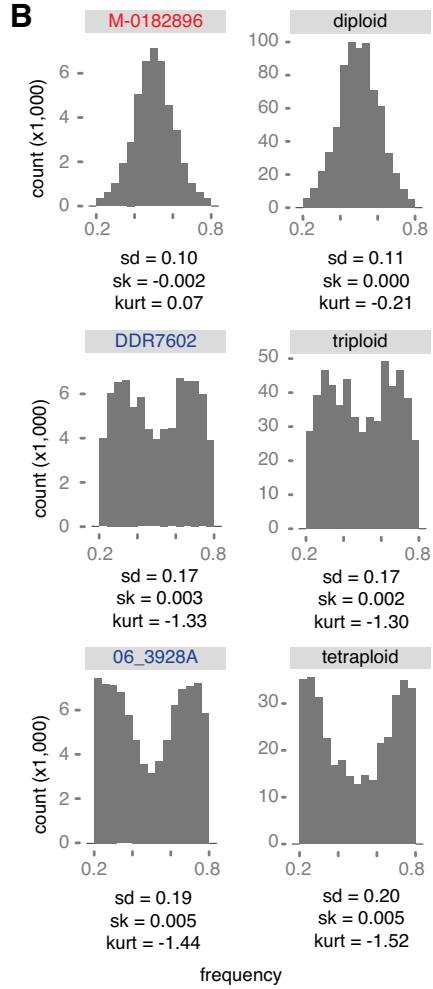
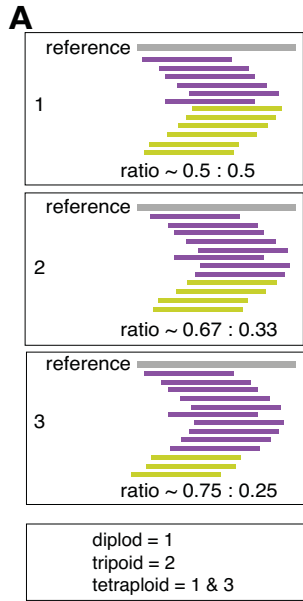


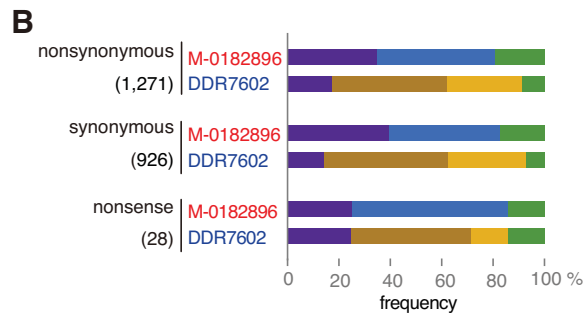
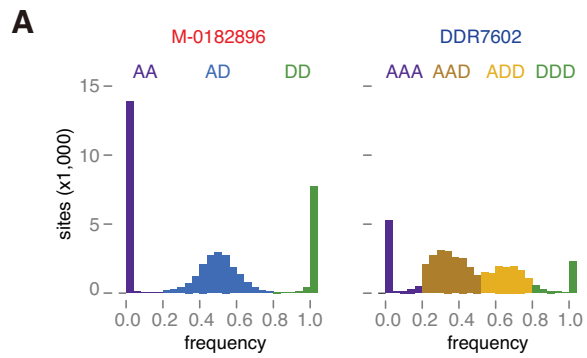


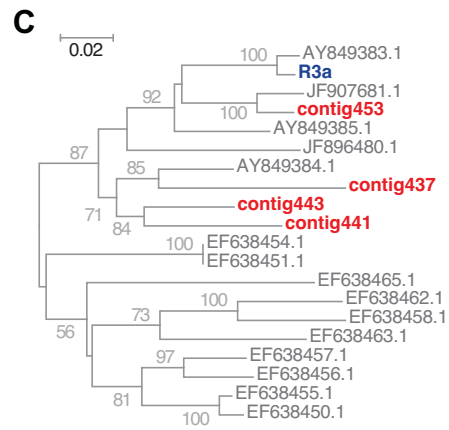
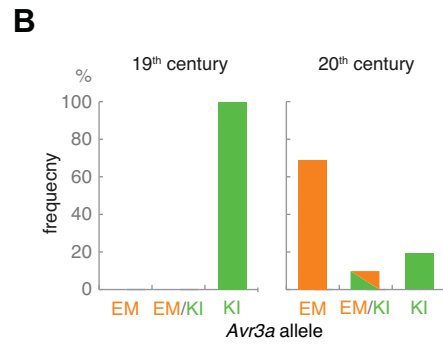
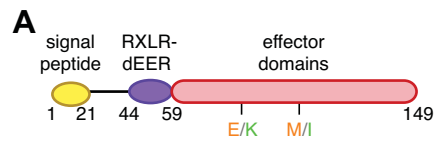


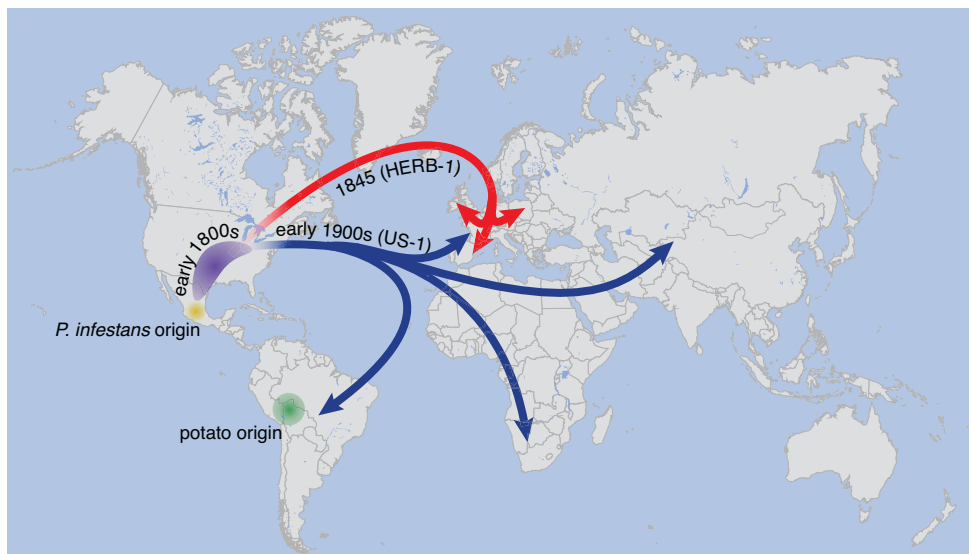


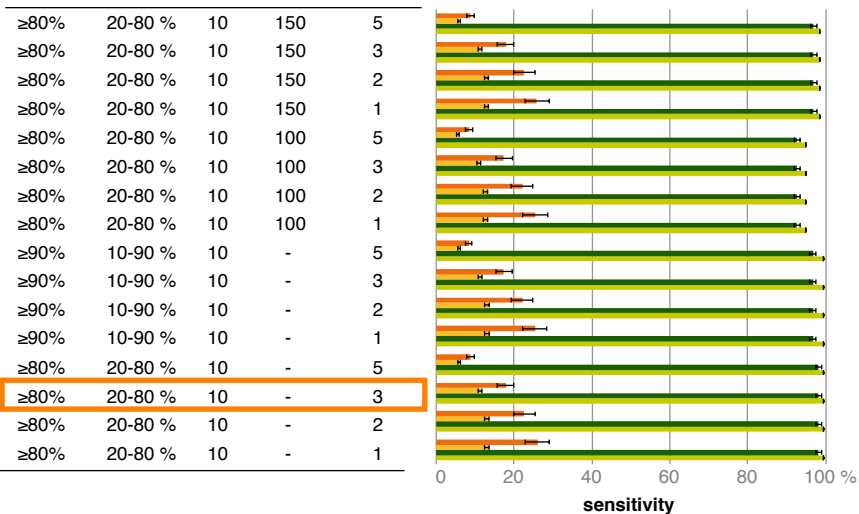
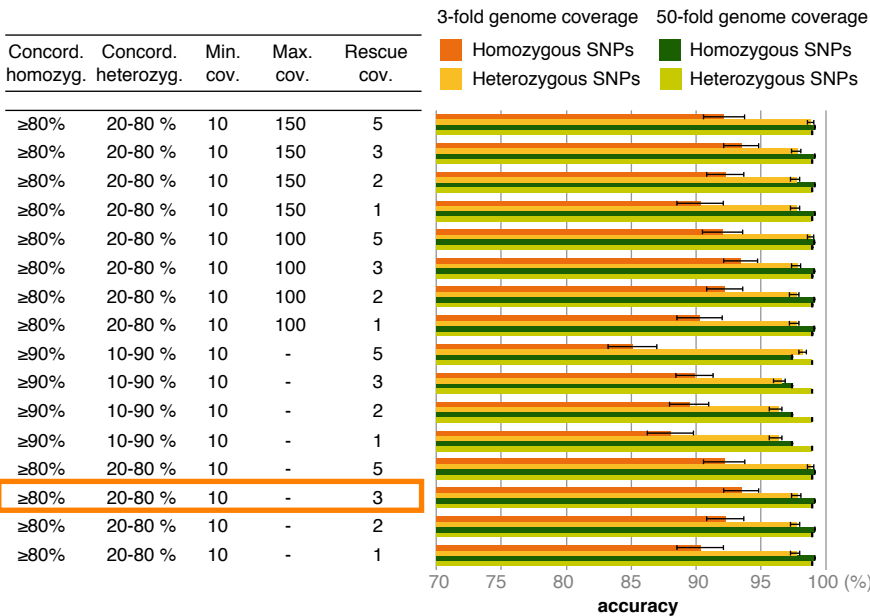


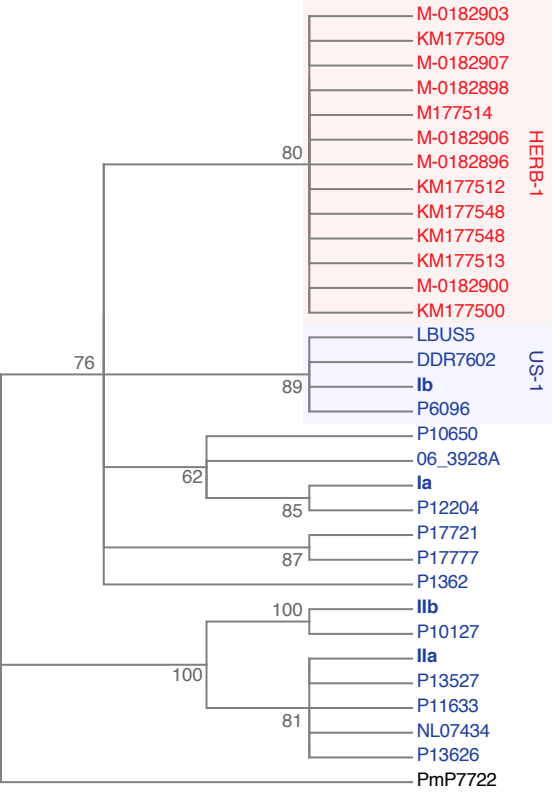




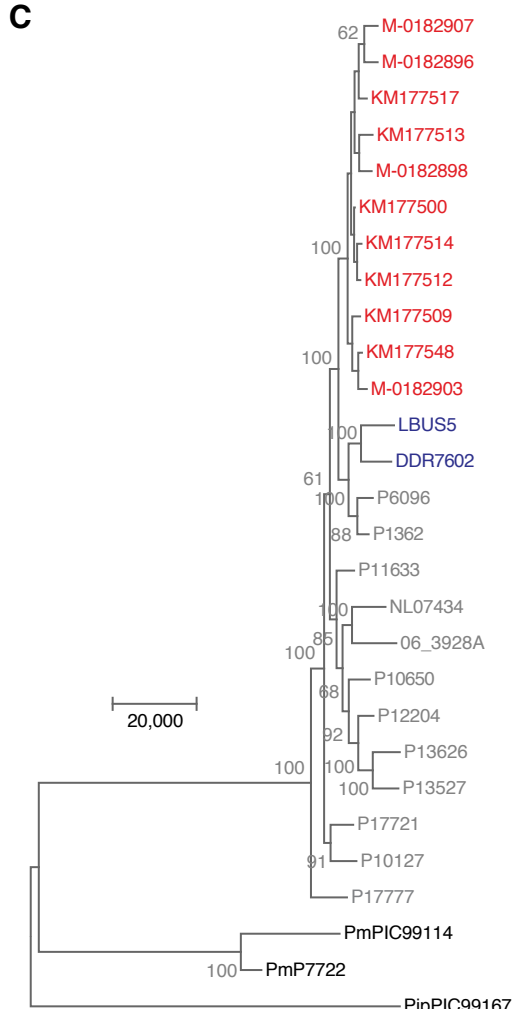
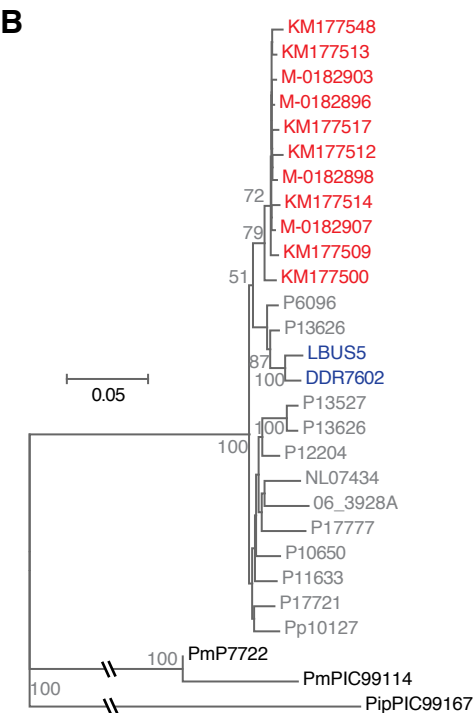
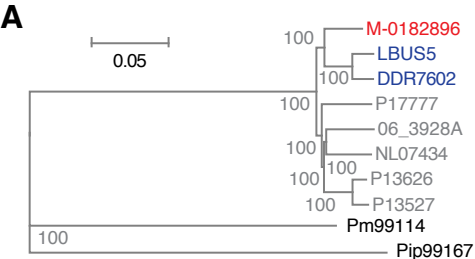


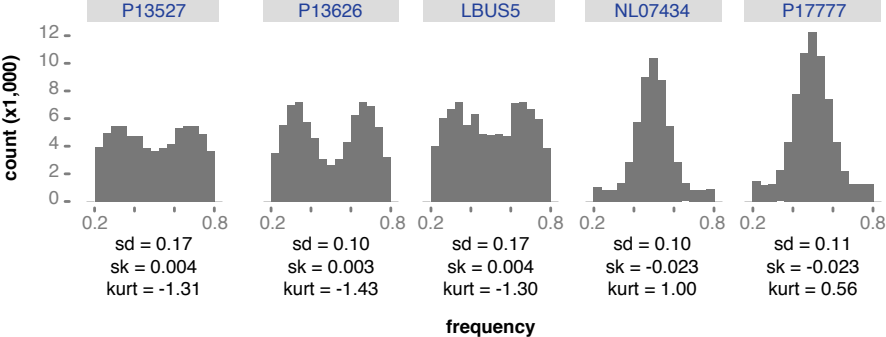






la	AATTTCTCCAACAAAAC TACTTGAACCTGG AATAGACATATTTGCTAATACATAAAATAA
lb	AATTTCTCCAACAAAAC TACTTGAACCCGG AATAGACATATTTGCTAATACATAAAATAA
IIa	AATTTCTCCAACAAAAC TACTTGAACCTGG AATAGACATATTTGCTAATACATAAAATAA
IIb	AATTTCTCCAACAAAAC TACTTGAACCTGG AATAGACATATTTGCTAATACATAAAATAA
M-0182898	AATTTCTCCAACAAAAC TACTTGAACCTGG AATAGACATATTTGCTAATACATAAAATAA
M-0182906	AATTTCTCCAACAAAAC TACTTGAACCTGG AATAGACATATTTGCTAATACATAAAATAA
M-0182907	AATTTCTCCAACAAAAC TACTTGAACCTGG AATAGACATATTTGCTAATACATAAAATAA
M-0182896	AATTTCTCCAACAAAAC TACTTGAACCTGG AATAGACATATTTGCTAATACATAAAATAA
M-0182903	AATTTCTCCAACAAAAC TACTTGAACCTGG AATAGACATATTTGCTAATACATAAAATAA
M-0182900	AATTTCTCCAACAAAAC TACTTGAACCTGG AATAGACATATTTGCTAATACATAAAATAA
KM177513	AATTTCTCCAACAAAAC TACTTGAACCTGG AATAGACATATTTGCTAATACATAAAATAA
KM177509	AATTTCTCCAACAAAAC TACTTGAACCTGG AATAGACATATTTGCTAATACATAAAATAA
KM177514	AATTTCTCCAACAAAAC TACTTGAACCTGG AATAGACATATTTGCTAATACATAAAATAA
KM177500	AATTTCTCCAACAAAAC TACTTGAACCTGG AATAGACATATTTGCTAATACATAAAATAA
KM177512	AATTTCTCCAACAAAAC TACTTGAACCTGG AATAGACATATTTGCTAATACATAAAATAA
KM177548	AATTTCTCCAACAAAAC TACTTGAACCTGG AATAGACATATTTGCTAATACATAAAATAA
KM177517	AATTTCTCCAACAAAAC TACTTGAACCTGG AATAGACATATTTGCTAATACATAAAATAA





kmer	N50 (bp)	Longest Contig (bp)	RXLR proteins with TBLASTN hit	AVR1	AVR2	AVR3a ^{EM}	AVR4
41	160	2,686	25	48	81	37	66
51	169	4,616	61	39	100	46	78
61	191	8,487	89	100	100	84	87
63	219	9,428	90	77	100	84	87
65	241	9,430	92	100	99	84	87
67	248	9,509	90	100	99	97	79
69	257	15,874	88	100	99	97	79
71	259	14,583	76	100	91	97	45
81	312	36,586	76	100	99	97	45
91	362	73,532	48	75	79	90	44
101	393	68,999	19	75	79	90	7
111	429	68,999	15	75	65	69	7
121	473	25,791	6	7	8	51	7

Matched aa / AVR length (%)



0 50 100